

Two-dimensional fractional Brownian motion: Analysis in time and frequency domains

Michał Balcerek,¹ Adrian Pacheco-Pozo,^{2,3} Agnieszka Wyłomańska,¹ Krzysztof Burnecki,¹ and Diego Krapf^{2,3}

¹*Faculty of Pure and Applied Mathematics, Hugo Steinhaus Center, Wrocław University of Science and Technology, 50-370 Wrocław, Poland^{a)}*

²*Department of Electrical and Computer Engineering, Colorado State University, Fort Collins, CO 80523, USA*

³*School of Biomedical and Chemical Engineering, Colorado State University, Fort Collins, CO 80523, USA*

This article introduces a novel construction of the two-dimensional fractional Brownian motion (2D fBm) with dependent components. Unlike similar models discussed in the literature, our approach uniquely accommodates the full range of model parameters and explicitly incorporates cross-dependencies and anisotropic scaling through a matrix-valued Hurst operator. We thoroughly analyze the theoretical properties of the proposed causal and well-balanced 2D fBm versions, deriving their auto- and cross-covariance structures in both time and frequency domains. In particular, we present the power spectral density of these processes and their increments. Our analytical findings are validated with numerical simulations. This work provides a comprehensive framework for modeling anomalous diffusion phenomena in multidimensional systems where component interdependencies are crucial.

Keywords: 2D fBm, vector fractional Brownian motion, power spectral density, cross spectral density, multivariate self-similar processes, autocorrelation function, cross-correlation function

Two-dimensional fractional Brownian motion extends the idea of random motion by allowing both long-term memory and interdependence between different directions of movement. Unlike standard models, where the horizontal and vertical components are assumed to fluctuate independently, this process accounts for correlations and directional differences in scaling. We introduce these features through correlated underlying noises and the matrix-valued Hurst operator, which both make it possible for one direction to show, for example, slower subdiffusive dynamics while the other exhibits faster, superdiffusive behavior. We also show that, depending on how we choose to construct the process, the cross-correlations between components may be symmetric or asymmetric, leading to different temporal and spectral characteristics. The considered model is especially relevant for systems where anisotropy and interdependence cannot be ignored, such as the motion of particles in complex biological environments, the joint evolution of financial indices, or, simply, two correlated fractional Brownian motions.

^{a)}Electronic mail: michal.balcerek@pwr.edu.pl

I. INTRODUCTION

The study of anomalous diffusion phenomena has emerged as a critical area of research in diverse scientific fields, from cellular biophysics to financial mathematics¹⁻⁷. While standard Brownian motion adequately describes normal diffusion processes characterized by a mean-square displacement that increases linearly with time⁸, multiple complex systems exhibit a non-linear scaling that demands a more sophisticated mathematical framework¹. Fractional Brownian motion (fBm) originates from the foundational work of Kolmogorov in the 1940s, who first formulated a Gaussian process with stationary increments and a power-law covariance structure⁹. It was later formalized by Mandelbrot and van Ness, who introduced the integral representation and the Hurst parameter H as a descriptor of memory and anomalous scaling¹⁰. However, when considering multidimensional systems, the scalar parameter H can be insufficient to capture the complex cross-dependencies and anisotropic scaling behaviors observed in empirical data. Multidimensional fBm or vector fBm¹¹⁻¹⁴, thus, represents an advancement in the modeling of such anomalous diffusion processes in multidimensional settings.

A common approach to modeling multidimensional fBm involves treating each spatial component as an independent random walk. This strategy has been employed in a variety of contexts, including the analysis of diffusion in living cells and complex fluids, where isotropic behavior is often assumed over the observation timescales¹⁵⁻¹⁸. For instance, models with independent fBm components have been used to characterize anomalous transport of membrane proteins¹⁵, analyze motion changes in single-particle trajectories¹⁸, and assess spectral properties of anomalous diffusion processes^{17,18}. While this approach is well justified in systems where anisotropies are either negligible or not detectable within the experimental resolution, it becomes insufficient in environments where directional dependence or cross-correlations play a significant role. In such cases, assuming independence between components can obscure critical features of the dynamics and lead to misinterpretations. This motivates the development of models that explicitly incorporate cross-dependencies and anisotropic scaling.

While one expects many biophysical systems to be isotropic¹⁹⁻²¹, this is not the case when underlying structures have an inherent orientation. In such systems, a tracer may display a different scaling behavior along each spatial dimension and it is necessary to consider the interdependence among the different components. For example, anisotropic scalings emerge in the dynamics of proteins on the cell surface due to the presence of stress fibers²² and actin filaments²³, ions in the brain^{24,25}, macromolecules in the nucleocytoplasm during cell division²⁶, and species in rocks²⁷. Beyond physical systems, financial markets often exhibit non-uniform behavior, prompting the use of multivariate models to capture the joint dynamics of multiple assets or economic indicators²⁸. These models help in risk management, option pricing, and forecasting^{29,30}. Multidimensional models that allow dependencies between components have been covered in the literature. Notable examples include multidimensional Brownian motion^{28,31-35} and multidimensional Ornstein-Uhlenbeck processes^{33,36}. Previous discussions also extended to discrete-time models with dependent components, such as vector autoregressive time series³⁷⁻⁴⁰, or multidimensional generalized autoregressive conditional heteroskedasticity (GARCH) models⁴¹⁻⁴³.

In this article, we propose the construction of a two-dimensional fractional Brownian motion (2D fBm) by introducing a dependence on the underlying noise in the time representation of the process. This construction explicitly considers cross-dependencies and anisotropic

scaling by using a matrix-valued Hurst operator that allows direction-dependent scaling properties. Depending on the construction of the 2D fBm, we consider two versions of this process: causal and well-balanced. The well-balanced process is time-reversible, a property absent in the causal 2D fBm. As a result, these two formulations exhibit distinct correlation structures: symmetric cross-correlations for the well-balanced case and asymmetric cross-correlations for the causal case. We examine the theoretical properties of the two versions of 2D fBm and derive the auto- and cross-covariance structures of such process and their increments. In addition, we calculate the power spectral density (PSD) of these processes⁴⁴, a fundamental measure often used in the characterization of time series across different disciplines^{45–49}. At last, we present numerical simulations that showcase and validate our analytical results. Although multidimensional fBm with dependent components has been investigated in the existing literature^{14,37}, our proposition has the advantage of having a relatively simple construction, based on the correlated Brownian motions used in its integral representation. The new approach uniquely allows for any range of model parameters, a significant advantage over the previous constructions¹⁴. Consequently, this simplified construction enables a thorough examination of the process characteristics, particularly with respect to its auto- and cross-covariance structures in both the time and frequency domains.

The remainder of the paper is organized as follows. In [section II](#), we introduce the 2D fBm and discuss its two versions, namely causal and well-balanced. Next, in [section III](#), we analyze the covariance structure of 2D fBm and its increments, demonstrating the differences for causal and well-balanced cases. In [section IV](#), we analyze the covariance structure of 2D fBm and the corresponding increments in the frequency domain. In [section V](#) we present numerical simulations, while the last section contains conclusions. In the Appendix, we present additional calculations and plots.

II. MODEL

In this section, we propose two specific constructions of the 2D fBm, which serve as a mathematical tool for modeling anomalous diffusion processes in multidimensional spaces. Unlike the classical one-dimensional case, which relies on scalar parameters to characterize diffusion behavior, we employ a matrix-valued H to capture directional dependencies and cross-dimensional correlations. While we only consider the two-dimensional case, the extension to higher dimensions is straightforward. First, following Stoev and Taqqu⁵⁰, let us introduce the following function

$$f_{\pm}(x; t, \beta) = (t - x)_{\pm}^{\beta} - (-x)_{\pm}^{\beta}, \quad (1)$$

where the notation $(x)_{+}$ denotes the positive part of x , i.e.,

$$(x)_{+} \equiv \begin{cases} x, & \text{if } x > 0, \\ 0, & \text{if } x \leq 0, \end{cases} \quad (2)$$

and $(x)_{-}$ denotes the negative part of x , i.e., $(x)_{-} = (-x)_{+}$. Let us consider the two-dimensional process $\mathbf{X}(t) = [X_1(t), X_2(t)]'$, $t \geq 0$, defined as follows

$$\begin{cases} X_1(t) &= \sigma_1 a_{H_1} \int_{-\infty}^{\infty} f_{+}(s; t, H_1 - 1/2) d\tilde{W}_1(s), \\ X_2(t) &= \sigma_2 a_{H_2} \int_{-\infty}^{\infty} f_{+}(s; t, H_2 - 1/2) d\tilde{W}_2(s). \end{cases} \quad (3)$$

A similar alternative $\mathbf{X}^*(t) = [X_1^*(t), X_2^*(t)]', t \geq 0$, utilizing both f_+ and f_- is given by

$$\begin{cases} X_1^*(t) &= \sigma_1 a_{H_1}^* \int_{-\infty}^{\infty} (f_+(s; t, H_1 - 1/2) + f_-(s; t, H_1 - 1/2)) d\tilde{W}_1(s), \\ X_2^*(t) &= \sigma_2 a_{H_2}^* \int_{-\infty}^{\infty} (f_+(s; t, H_2 - 1/2) + f_-(s; t, H_2 - 1/2)) d\tilde{W}_2(s). \end{cases} \quad (4)$$

In both cases, $d\tilde{W}_1(t), d\tilde{W}_2(t)$ are ρ -correlated Gaussian noises on the real line, $H_1, H_2 \in (0, 1)$, and $\sigma_1, \sigma_2 > 0$. The constants $a_{H_1}, a_{H_2}, a_{H_1}^*$, and $a_{H_2}^*$ are chosen in such a way that the processes $X_j(t)$ and $X_j^*(t)$ for $j = 1, 2$ have variances σ_1^2 and σ_2^2 for $t = 1$, respectively, that is, $\langle X_j^2(1) \rangle = \langle X_j^{*2}(1) \rangle = \sigma_j^2$, for $j = 1, 2$. Parameter ρ will be referred to as correlation coefficient of the underlying noise. Let us note that for both processes $\mathbf{X}(t)$ and $\mathbf{X}^*(t)$, the marginals $X_j(t)$ and $X_j^*(t)$ ($j = 1, 2$) are fractional Brownian motions with corresponding Hurst parameters H_j (cf.¹⁰ for $\mathbf{X}(t)$ and⁵⁰ for $\mathbf{X}^*(t)$). The difference between the seemingly similar processes $\mathbf{X}(t)$ and $\mathbf{X}^*(t)$ lies in the cross-dependence structure between their components, specifically between $X_1(t)$ and $X_2(t)$, and between $X_1^*(t)$ and $X_2^*(t)$, respectively, which we discuss in the next section.

To establish the connection between the processes $\mathbf{X}(t)$ and $\mathbf{X}^*(t)$ and the vector fractional Brownian motion discussed in the literature^{14,51,52}, let us consider two independent Brownian motions $W_1(t), W_2(t)$ on the real line and define $\tilde{W}_1(t)$ and $\tilde{W}_2(t)$ in the following way

$$\begin{cases} \tilde{W}_1(t) = W_1(t) \\ \tilde{W}_2(t) = \rho W_1(t) + \sqrt{1 - \rho^2} W_2(t). \end{cases} \quad (5)$$

One can easily show that such a construction leads to $\langle d\tilde{W}_1(t) d\tilde{W}_2(t) \rangle = \rho dt$. Using the construction from Eq. (5), the processes defined in Eqs. (3) and (4) can be represented more concisely, as shown in the following definitions. Note that the adjectives ‘causal’ and ‘well-balanced’ in the processes’ names are already established in the literature. We follow this convention throughout the article.

Definition 1 (Causal 2D fBm). *Let $H_1, H_2 \in (0, 1)$ and $|\rho| \leq 1$. Causal two-dimensional fractional Brownian motion $\mathbf{X}(t), t \geq 0$, is defined via the following integral representation*

$$\mathbf{X}(t) = \int_{-\infty}^{\infty} \begin{bmatrix} \sigma_1 a_{H_1} f_+(s; t, H_1 - 1/2) & 0 \\ 0 & \sigma_2 a_{H_2} f_+(s; t, H_2 - 1/2) \end{bmatrix} \begin{bmatrix} 1 & 0 \\ \rho & \sqrt{1 - \rho^2} \end{bmatrix} \begin{bmatrix} dW_1(s) \\ dW_2(s) \end{bmatrix}, \quad (6)$$

where $\sigma_1, \sigma_2 > 0$. The constants $a_{H_j}, j = 1, 2$ are non-negative, and are chosen in such a way that the variances of the marginals $X_j(t)$ at time $t = 1$ are equal to σ_j^2 , i.e.,

$$a_{H_j}^2 = \frac{\Gamma(2H_j + 1) \sin(H_j \pi)}{\Gamma^2(H_j + \frac{1}{2})}. \quad (7)$$

The process $\mathbf{X}(t)$ is a zero-mean Gaussian process and has a strong connection to the so-called operator fractional Brownian motion⁵²⁻⁵⁵. Such a relation allows for analyzing the covariance structure of the process $\mathbf{X}(t)$ (see [Theorem 1](#) in [section III](#)).

Remark 1. *Let us notice that the marginals $X_j(t), j = 1, 2$ of the causal 2D fBm follow the well-known Mandelbrot and van Ness definition¹⁰ of fBm, i.e.,*

$$X_j(t) = \sigma_j a_{H_j} \int_{-\infty}^t \left((t-s)_+^{H_j - \frac{1}{2}} - (-s)_+^{H_j - \frac{1}{2}} \right) d\tilde{W}_j(s), \quad \text{for } j = 1, 2. \quad (8)$$

Contrary to the causal construction presented in Definition 1, the well-balanced case adds to the previous case an anti-causal filtering of a Brownian motion. We now introduce such a process, together with the calculation of the normalization constant (Theorem 6 in Appendix section B). The covariance structure of well-balanced 2D fBm is provided in section III.

Definition 2 (Well-balanced 2D fBm). *Let $H_1, H_2 \in (0, 1)$ and $|\rho| \leq 1$. Well-balanced two-dimensional fractional Brownian motion $\mathbf{X}^*(t)$ is given by the following representation*

$$\mathbf{X}^*(t) = \int_{-\infty}^{\infty} \begin{bmatrix} g_1(s; t) & 0 \\ 0 & g_2(s; t) \end{bmatrix} \begin{bmatrix} 1 & 0 \\ \rho & \sqrt{1 - \rho^2} \end{bmatrix} \begin{bmatrix} dW_1(s) \\ dW_2(s) \end{bmatrix}, \quad (9)$$

where

$$g_j(s; t) = \sigma_j a_{H_j}^* (f_+(s; t, H_j - 1/2) + f_-(s; t, H_j - 1/2)) \quad (10)$$

for $s \in \mathbb{R}, t \geq 0, j = 1, 2, \sigma_1, \sigma_2 > 0$, and the constants $a_{H_j}^*$ are given by

$$a_H^{*2} = \frac{2H(1 - 2H)\pi}{8\Gamma(2 - 2H) \cos(H\pi)\Gamma^2(H + 1/2) \cos^2\left(\frac{\pi(H - 1/2)}{2}\right)}, \quad (11)$$

to ensure the variances of the marginals $X_j^*(t)$ at time $t = 1$ are equal to σ_j^2 .

Similarly to the causal 2D fBm, the well-balanced 2D fBm is a zero-mean Gaussian process.

The proposed constructions of 2D fBm are closely related to the general operator fractional Brownian motion (OFBM), a family of processes even more general than vector fractional Brownian motion. OFBM is a multivariate Gaussian process defined through a matrix-valued self-similarity exponent and integral kernels acting on multidimensional Brownian noise^{52–55}. This connection provides helpful tools for the presented models and situates them within the broader theory of multivariate self-similar processes.

Both of our considered models coincide with OFBM with the exponent matrix $D = \text{diag}(H_1 - \frac{1}{2}, H_2 - \frac{1}{2})$ and a kernel matrix determined by correlation parameter of the underlying noise ρ and the model itself. Since in the causal 2D fBm the negative-time kernel is absent, the resulting process is inherently asymmetric in time. In contrast, the well-balanced 2D fBm corresponds to an OFBM with both positive and negative kernels present in a symmetric manner, resulting in a time-reversible process. This structural distinction is discussed in section III and is described through the asymmetry parameter η_{12} .

While OFBM theory typically imposes nontrivial admissibility conditions on the exponent and kernel matrices, our presented construction avoids these difficulties by employing correlated Brownian motions directly in the integral representation. As a consequence, the model is valid for all $H_1, H_2 \in (0, 1)$ and $|\rho| \leq 1$ without additional constraints. Thus, the introduced 2D fBm may be viewed as a subclass of OFBM, one that naturally captures both symmetric and asymmetric cross-dependence through the choice of causal or well-balanced form of integral kernels.

III. COVARIANCE STRUCTURE OF 2D FBM

In this section, we discuss the covariance structure of both causal and well-balanced 2D fBms, along with that of their increments.

A. Covariance structure of the process

As mentioned, both causal and well-balanced 2D fBm are Gaussian processes; therefore, their covariance structure provides a complete characterization. In this section, we discuss this characterization in time domain.

Theorem 1. *Let $H_1, H_2 \in (0, 1)$ and $|\rho| \leq 1$. The covariance structure of 2D fBm $\mathbf{Z}(t) = [Z_1(t), Z_2(t)]'$, $t \geq 0$ is as follows*

$$\gamma_{jk}(t, s) \equiv \langle Z_j(t)Z_k(s) \rangle = \frac{\sigma_j \sigma_k}{2} (w_{jk}(t)|t|^{H_j+H_k} + w_{jk}(-s)|s|^{H_j+H_k} - w_{jk}(t-s)|t-s|^{H_j+H_k}) \quad (12)$$

for $t, s \geq 0$, where $\sigma_j^2 = \langle Z_j^2(1) \rangle$ and

$$w_{jk}(u) = \begin{cases} \rho_{jk} - \eta_{jk} \text{sign}(u), & H_j + H_k \neq 1, \\ \rho_{jk} - \eta_{jk} \text{sign}(u) \log |u|, & H_j + H_k = 1. \end{cases} \quad (13)$$

The, so called, cross-correlation parameters ρ_{12} and ρ_{21} are given by

$$\rho_{12} = \rho_{21} = \rho \frac{\sqrt{\Gamma(2H_1+1)\Gamma(2H_2+1)\sin(H_1\pi)\sin(H_2\pi)}}{\Gamma(H_1+H_2+1)\sin\left(\frac{H_1+H_2}{2}\pi\right)} \cos\left[\frac{(H_2-H_1)\pi}{2}\right], \quad (14)$$

and $\rho_{11} = \rho_{22} = 1$ while the asymmetry parameters η_{jk} , $j, k = 1, 2$, depend on the choice of the model, and in the causal 2D fBm (case $\mathbf{Z}(t) = \mathbf{X}(t)$) they are equal to

$$\eta_{12} = -\eta_{21} = \rho \frac{\sqrt{\Gamma(2H_1+1)\Gamma(2H_2+1)\sin(H_1\pi)\sin(H_2\pi)}}{\Gamma(H_1+H_2+1)\cos\left(\frac{H_1+H_2}{2}\pi\right)} \sin\left[\frac{(H_2-H_1)\pi}{2}\right], \quad (15)$$

and $\eta_{11} = \eta_{22} = 0$, while for well-balanced 2D fBm (case $\mathbf{Z}(t) = \mathbf{X}(t)^*$) we have

$$\eta_{11} = \eta_{22} = \eta_{12} = \eta_{21} = 0. \quad (16)$$

Proof. The proof of this theorem is presented in Appendix [section A](#) and Appendix [section C](#). \square

Remark 2. *Since for well-balanced 2D fBm $\eta_{jk} = 0$ for $j, k = 1, 2$, the covariance function simplifies remarkably. Similar to one-dimensional fBm, it is given by*

$$\gamma_{jk}(t, s) = \frac{\sigma_j \sigma_k \rho_{jk}}{2} (|t|^{H_j+H_k} + |s|^{H_j+H_k} - |t-s|^{H_j+H_k}). \quad (17)$$

Remark 3. *Let us note that for $H_1 = H_2$ both causal and well-balanced 2D fBms define the same process. For $H_1 = H_2 = 0.5$, both constructions lead to 2D Brownian motion with ρ correlated coordinates²⁸.*

Remark 4. *Let us observe that ρ_{12} given in Eq. (14) can be expressed as*

$$\rho_{12} = \langle Z_1(1)Z_2(1) \rangle / \sqrt{\langle Z_1^2(1) \rangle \langle Z_2^2(1) \rangle}, \quad (18)$$

that is, it plays the role of the cross-correlation coefficient of $\mathbf{Z}(t)$ at time $t = 1$.

Theorem 1 highlights the primary distinction between the two considered models. For the causal 2D fBm, we observe that when $\eta_{12} \neq 0$, the cross-covariance function $\gamma_{12}(s, t)$ is asymmetric, meaning $\gamma_{12}(s, t) \neq \gamma_{12}(t, s)$. This is in contrast to the marginal processes, for which $\gamma_{jj}(s, t) = \gamma_{jj}(t, s)$ for any suitable choice of distinct times t and s . Conversely, for well-balanced 2D fBm, the cross-covariance function is symmetric (because $\eta_{12} = \eta_{21} = 0$).

The correspondence between the correlation coefficient of the underlying noise ρ and the cross-correlation of the process, ρ_{12} , presented in Eq. (14), is shown in Figure 1(a) for different Hurst parameter pairs (H_1, H_2) of the coordinates $X_1(t)$ and $X_2(t)$. Let us highlight the fact that, when the difference between H_1 and H_2 is large (e.g., $H_1 = 0.2, H_2 = 0.7$, yellow line in the figure) the resulting cross-correlation range is much smaller than the correlation of the underlying noise. In the extreme case of $|\rho| = 1$, the parameter $|\rho_{12}| \approx 0.5$. When the difference between H_1 and H_2 is small (e.g., $|H_1 - H_2| = 0.25 \pm 0.05$, orange and violet lines in the figure), the resulting ρ_{12} is similar to the correlation ρ .

The correspondence between ρ and the asymmetry parameter η_{12} , as given in Eq. (15), is presented in Figure 1(b). We observe that η_{12} increases with the difference between H_1 and H_2 , while ρ_{12} decreases.

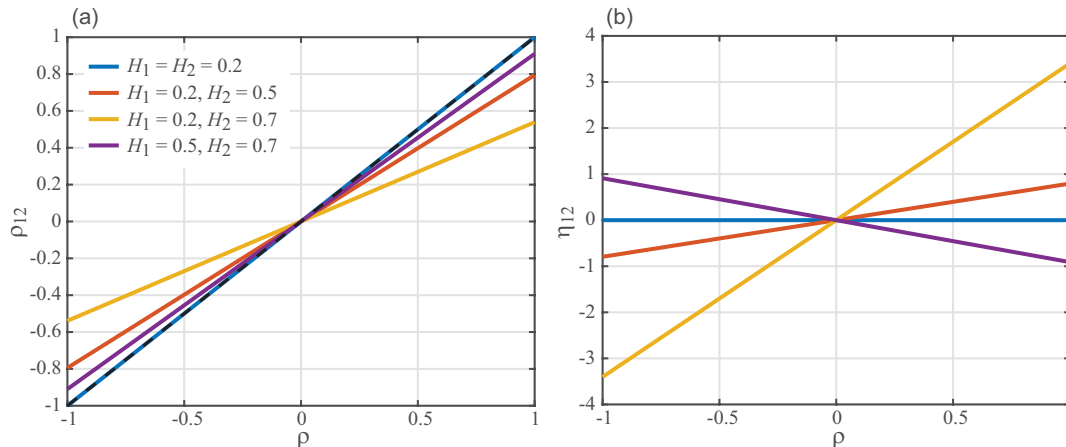


FIG. 1. The dependence between correlation ρ of the underlying noise and (a) cross-correlation coefficient ρ_{12} and (b) asymmetry parameter η_{12} of the process $\mathbf{X}(t)$ and $\mathbf{X}^*(t)$. Different solid lines correspond to different Hurst exponents of the coordinates, while the black dashed line corresponds to the identity cases $\rho_{12} = \rho$ or $\eta_{12} = \rho$, shown as a guide to the eye.

Remark 5. Under the presented construction, the introduced processes $\mathbf{X}(t)$ and $\mathbf{X}^*(t)$ are well-defined for all sets of parameters $H_1, H_2 \in (0, 1)$ and $|\rho| \leq 1$. Such a natural construction ensures that the condition given in Remark 8 in¹⁴ is true. Moreover, we see that $\rho_{12}^2 \leq \rho^2$.

B. Covariance structure of increments

For any process $\mathbf{Z}(t)$, the increment process over a step $\delta > 0$ is defined as

$$\Delta^\delta \mathbf{Z}(t) \equiv \mathbf{Z}(t + \delta) - \mathbf{Z}(t). \quad (19)$$

In the following theorem, we present the covariance structure for the increment process of the causal and well-balanced 2D fBm.

Theorem 2. Let $H_1, H_2 \in (0, 1)$ and $|\rho| \leq 1$. The covariance structure of the increment process $\Delta^\delta \mathbf{Z}(t)$ of causal or well-balanced 2D fBm is as follows

$$\begin{aligned} \gamma_{jk}^\Delta(t, s) = \langle \Delta^\delta Z_j(t) \Delta^\delta Z_k(s) \rangle &= \frac{\sigma_j \sigma_k \rho_{jk}}{2} [w_{jk}(t-s+\delta)|t-s+\delta|^{H_j+H_k} \\ &+ w_{jk}(t-s-\delta)|t-s-\delta|^{H_j+H_k} - 2w_{jk}(t-s)|t-s|^{H_j+H_k}], \end{aligned} \quad (20)$$

where the function w_{jk} is given in Eq.(13) and depends on whether we consider causal or well-balanced 2D fBm. The coefficients ρ_{jk} and η_{jk} are defined in Theorem 1.

Proof. The proof of this theorem is a natural consequence of the covariance structure of the introduced processes $\mathbf{X}(t)$ and $\mathbf{X}^*(t)$. For the increment process of the causal 2D fBm $\mathbf{X}(t)$ we have

$$\begin{aligned} \langle \Delta^\delta X_j(t) \Delta^\delta X_k(s) \rangle &= \langle (X_j(t+\delta) - X_j(t))(X_k(s+\delta) - X_k(s)) \rangle \\ &= \gamma_{jk}(t+\delta, s+\delta) - \gamma_{jk}(t, s+\delta) - \gamma_{jk}(t+\delta, s) + \gamma_{jk}(t, s), \quad j, k = 1, 2. \end{aligned} \quad (21)$$

Substituting the covariance function γ_{jk} using the results of Theorem 1 yields the desired covariance structure of the increment process. The proof for well-balanced 2D fBm is analogous. \square

Let us note that for both considered processes, the covariance structure depends only on $h = t - s$ and the length of the interval δ on which the increments are taken. For $j = k$, we retain the autocovariance function of fractional Brownian motion corresponding to that coordinate⁵⁶, i.e.,

$$\langle \Delta^\delta X_j(t) \Delta^\delta X_j(s) \rangle = \langle \Delta^\delta X_j^*(t) \Delta^\delta X_j^*(s) \rangle = \frac{\sigma_j^2}{2} (|t-s+\delta|^{2H_j} + |t-s-\delta|^{2H_j} - 2|t-s|^{2H_j}). \quad (22)$$

IV. SPECTRAL CONTENT

The PSD matrix plays a central role in the analysis of multidimensional stochastic processes⁵⁷. This quantity generalizes the concept of a PSD to vector-valued processes. It is particularly valuable in multiple fields, including econometrics⁵⁸, structural engineering^{59,60}, neuroscience⁶¹, and signal processing⁶², where complex systems exhibit interactions across multiple channels or variables. Since PSD is more frequently employed in the context of stationary processes, we begin this section by analyzing the increments of 2D fBm.

A. Spectral content of the increments

In the multivariate setting, for any second-order stationary process $\Delta \mathbf{Z}(t)$, $t \geq 0$, we can consider the power spectral density matrix $S_{\Delta \mathbf{Z}}(f)$ of a single realization

$$S_{\Delta \mathbf{Z}}(f) = \lim_{T \rightarrow \infty} \frac{1}{T} \int_0^T \int_0^T e^{i(t-s)f} \Delta \mathbf{Z}(t) \Delta \mathbf{Z}(s)' dt ds, \quad f \in \mathbb{R}, \quad (23)$$

with ensemble average

$$\langle S_{\Delta \mathbf{Z}}(f) \rangle = \lim_{T \rightarrow \infty} \frac{1}{T} \int_0^T \int_0^T e^{i(t-s)f} \gamma_{\Delta \mathbf{Z}}(t-s) dt ds, \quad f \in \mathbb{R}, \quad (24)$$

where $\gamma_{\Delta\mathbf{Z}}(n) = \langle \Delta\mathbf{Z}(n)\Delta\mathbf{Z}(0)' \rangle$ for the zero-mean process $\Delta\mathbf{Z}(t)$. Eq. (24) simplifies to

$$\langle S_{\Delta\mathbf{Z}}(f) \rangle = \int_{-\infty}^{\infty} e^{itf} \gamma_{\Delta\mathbf{Z}}(t) dt, \quad f \in \mathbb{R}, \quad (25)$$

which is known as Wiener-Khinchin theorem⁶³. Let us note, that for a d -dimensional process, the function $S_{\Delta\mathbf{Z}}$ is a $d \times d$ matrix with the diagonal elements corresponding to marginals and off-diagonal elements describing the, so called, cross power spectral density⁵⁷. To streamline the notation, we will use now S^Δ whenever PSD relates to the increments process, instead of using $S_{\Delta\mathbf{Z}}$.

One can also consider the components of a power spectral density matrix

$$\langle S_{jk}^\Delta(f) \rangle = \int_{-\infty}^{\infty} e^{itf} \gamma_{jk}^\Delta(t) dt, \quad f \in \mathbb{R}, \quad j, k = 1, 2. \quad (26)$$

It is worth noting that unlike the one-dimensional version of spectral density, the cross components S_{jk}^Δ for $j \neq k$ might not be real-valued. In general, it is true that $S_{jk}^\Delta(f) = \overline{S_{kj}^\Delta(f)}$ for all f 's, where \bar{z} denotes the complex conjugate of z .

Theorem 3. *Let $H_1, H_2 \in (0, 1)$, $H = \text{diag}(H_1, H_2)$ be a diagonal matrix with elements H_1, H_2 , and $|\rho| \leq 1$. Additionally, let matrices $C_c = [c_{jk}^c]_{j,k=1,2}$ and $C_{wb} = [c_{jk}^{wb}]_{j,k=1,2}$ that correspond to causal and well-balanced 2D fBm, respectively, have the following elements*

$$c_{jj}^c = \frac{1}{2\pi} \sigma_j^2 \Gamma^2(H_j + 0.5) a_{H_j}^2, \quad (27)$$

$$c_{jk}^c = \frac{1}{2\pi} \rho \sigma_j \sigma_k \Gamma(H_j + 0.5) \Gamma(H_k + 0.5) a_{H_j} a_{H_k} e^{-i\frac{\pi}{2}(H_j - H_k)}, \quad j \neq k, \quad (28)$$

$$c_{jj}^{wb} = \frac{2}{\pi} \sigma_j^2 \cos^2\left(\frac{(H_j - 0.5)\pi}{2}\right) \Gamma^2(H_j + 0.5) a_{H_j}^{*2}, \quad (29)$$

$$c_{jk}^{wb} = \frac{1}{2\pi} \rho \sigma_j \sigma_k \cos\left(\frac{(H_j - 0.5)\pi}{2}\right) \cos\left(\frac{(H_k - 0.5)\pi}{2}\right) \Gamma(H_j + 0.5) \Gamma(H_k + 0.5) a_{H_j}^* a_{H_k}^*, \quad j \neq k, \quad (30)$$

for $j, k = 1, 2$. Constants a_{H_j} and $a_{H_j}^*$ are given in Eqs. (7) and (11), respectively. Then, for the increments of 2D fBm the power spectral density matrix $S^\Delta(f)$ is given by

$$\langle S^\Delta(f) \rangle = |1 - e^{-if}|^2 \sum_{n=-\infty}^{\infty} \left[(f + 2\pi n)_+^{-D} \tilde{C} (f + 2\pi n)_+^{-D} + (f + 2\pi n)_-^{-D} \overline{\tilde{C}} (f + 2\pi n)_-^{-D} \right] / (f + 2\pi n)^2, \quad (31)$$

where $(x)_+ \equiv \max\{x, 0\}$, $(x)_- \equiv \max\{-x, 0\}$, $D = \text{diag}(H_1, H_2) - 0.5I_2$, I_2 is a 2×2 identity matrix, and $\overline{\tilde{C}}$ denotes the element-wise complex conjugate of matrix \tilde{C} . Matrix \tilde{C} is equal to C_c or C_{wb} depending if we consider causal or well-balanced 2D fBm. The components $\langle S_{jk}^\Delta \rangle$ can be thus expressed as

$$\langle S_{jk}^\Delta(f) \rangle = |1 - e^{-if}|^2 \sum_{n=-\infty}^{\infty} \left[(f + 2\pi n)_+^{1-H_j-H_k} \tilde{c}_{jk} + (f + 2\pi n)_-^{1-H_j-H_k} \overline{\tilde{c}_{jk}} \right] / (f + 2\pi n)^2, \quad (32)$$

where \tilde{c}_{jk} are elements of the appropriate matrix, C_c for the causal case or C_{wb} for the well-balanced one. Moreover, for $f \rightarrow 0$ we have

$$\langle S^\Delta(f) \rangle \sim f^{-D} \tilde{C} f^{-D}. \quad (33)$$

The element-wise asymptotic is as follows

$$\langle S_{jk}^\Delta(f) \rangle \sim \tilde{c}_{jk} f^{-(d_j+d_k)} = \tilde{c}_{jk} f^{-(H_j+H_k-1)}. \quad (34)$$

Proof. The proof of this theorem is presented in Appendix [section D](#). \square

Remark 6. Matrices C_c and C_{wb} given in [Theorem 3](#) have real elements on the diagonal, thus, $\langle S_{jj}^\Delta \rangle, j = 1, 2$, is also a real (and non-negative) function.

Remark 7. The direct derivation of matrix C given in [Theorem 3](#) be found in the proof of [Theorem 1](#) given in Appendix [section A](#) and Appendix [section C](#).

B. Spectral content of the process

An extension of PSD calculated on the stationary process (here, for the increments process of 2D fBm), one considers PSD calculated based on the information from the trajectory. In particular, given a nonstationary 1D process $Z(t)$, $0 \leq t \leq T$, measured over a time T , the PSD is typically defined as^{16,44,64,65}

$$S_Z(f, T) \equiv \frac{1}{T} \left| \int_0^T e^{ift} Z(t) dt \right|^2. \quad (35)$$

Note that in contrast to Eq. (23), the PSD depends on measurement time T . In d dimensions, the natural extension of the PSD defined in Eq. (35) for a real process $\mathbf{Z}(t)$, $0 \leq t \leq T$, can be written in an equivalent form,

$$S_{\mathbf{Z}}(f, T) = \frac{1}{T} \int_0^T e^{ift} \mathbf{Z}(t) dt \left(\int_0^T e^{ifs} \mathbf{Z}(s) ds \right)^*, \quad (36)$$

where $(\mathbf{x})^*$ is the Hermitian transpose (also known as the conjugate transpose) of \mathbf{x} , i.e., $(\mathbf{x})^* = \bar{\mathbf{x}}'$. Again, the function $S_{\mathbf{Z}}$ is a $d \times d$ matrix with the diagonal elements corresponding to marginals, and off-diagonal elements corresponding to the cross power spectral density. Eq. (36) can be written using a double integral

$$S_{\mathbf{Z}}(f, T) = \frac{1}{T} \int_0^T \int_0^T e^{if(t-s)} \mathbf{Z}(t) \mathbf{Z}'(s) ds dt. \quad (37)$$

Taking the expected value, we can also calculate the ensemble-averaged PSD

$$\langle S_{\mathbf{Z}}(f, T) \rangle \equiv \frac{1}{T} \int_0^T \int_0^T e^{if(t-s)} \langle \mathbf{Z}(t) \mathbf{Z}'(s) \rangle ds dt, \quad (38)$$

alternatively, written component-wise it is

$$\langle S_{\mathbf{Z},jk}(f, T) \rangle \equiv \frac{1}{T} \int_0^T \int_0^T e^{if(t-s)} \langle Z_j(t) Z_k(s) \rangle ds dt, \quad j, k = 1, 2. \quad (39)$$

Let us note that for $j = k$ we obtain the classical PSD given in Eq. (35) of the 1D process corresponding to the marginals. Here, we further use the simplified notation S_{jk} instead of $S_{\mathbf{Z},jk}$ to streamline the notation whenever it is clear which process is referred to. In both cases (causal and well-balanced), ensemble-averaged PSD for 2D fBm can be expressed as

$$\langle S_{jk}(\tilde{\omega}, T) \rangle = T^{H_j+H_k+1} \frac{\sigma_j \sigma_k}{2} \int_0^1 \int_0^1 e^{i\tilde{\omega}(t-s)} \left(w_{jk}(x) x^{H_j+H_k} + w_{jk}(-y) y^{H_j+H_k} - w_{jk}(x-y) |x-y|^{H_j+H_k} \right) dx dy, \quad (40)$$

where $\tilde{\omega} = fT$. The function w_{jk} is defined in Eq. (13) with parameters ρ_{jk} and asymmetry parameters η_{jk} defined in Theorem 1. In the following theorem, we present the behavior of such a function.

Theorem 4. *For the 2D fBm with $H_1 + H_2 \neq 1$, the ensemble-averaged PSD for coordinates $j, k = 1, 2$ has the form*

$$\langle S_{jk}(\tilde{\omega}, T) \rangle = T^{H_j + H_k + 1} \sigma_j \sigma_k \left\{ \rho_{jk} \left[\frac{1 - \cos \tilde{\omega}}{\tilde{\omega}} \mathcal{S}_{jk} - \left(1 - \frac{\sin \tilde{\omega}}{\tilde{\omega}} \right) \mathcal{C}_{jk} + \frac{d}{d\tilde{\omega}} \mathcal{S}_{jk} \right] + \eta_{jk} i \left[\frac{1 - \cos \tilde{\omega}}{\tilde{\omega}} \mathcal{C}_{jk} - \left(1 + \frac{\sin \tilde{\omega}}{\tilde{\omega}} \right) \mathcal{S}_{jk} - \frac{d}{d\tilde{\omega}} \mathcal{C}_{jk} \right] \right\}, \quad (41)$$

where

$$\mathcal{C}_{jk} \equiv \mathcal{C}_{jk}(\tilde{\omega}) = \int_0^1 \cos(\tilde{\omega}x) x^{H_j + H_k} dx, \quad (42)$$

$$\mathcal{S}_{jk} \equiv \mathcal{S}_{jk}(\tilde{\omega}) = \int_0^1 \sin(\tilde{\omega}x) x^{H_j + H_k} dx. \quad (43)$$

Parameters ρ_{jk} and η_{jk} are given in Theorem 1.

Proof. The proof of this theorem is included in Appendix section E. \square

Remark 8. *We can also use alternative forms for functions \mathcal{C} and \mathcal{S} defined in Eqs. (42) and (43), respectively, to obtain the expressions without derivatives. Alternatively, using integration by parts and the identities*

$$\frac{d}{d\tilde{\omega}} \mathcal{S}_{jk} = \frac{\sin \tilde{\omega}}{\tilde{\omega}} - \frac{H_j + H_k + 1}{\tilde{\omega}} \mathcal{S}_{jk}, \quad (44)$$

$$\frac{d}{d\tilde{\omega}} \mathcal{C}_{jk} = \frac{\cos \tilde{\omega}}{\tilde{\omega}} - \frac{H_j + H_k + 1}{\tilde{\omega}} \mathcal{C}_{jk}, \quad (45)$$

we obtain the equivalent expression

$$\langle S_{jk}(\tilde{\omega}, T) \rangle = T^{H_j + H_k + 1} \sigma_j \sigma_k \left\{ \rho_{jk} \left[\frac{1 - \cos \tilde{\omega} - H_j - H_k - 1}{\tilde{\omega}} \mathcal{S}_{jk} - \left(1 - \frac{\sin \tilde{\omega}}{\tilde{\omega}} \right) \mathcal{C}_{jk} + \frac{\sin \tilde{\omega}}{\tilde{\omega}} \right] + \eta_{jk} i \left[\frac{1 - \cos \tilde{\omega} + H_j + H_k + 1}{\tilde{\omega}} \mathcal{C}_{jk} - \left(1 + \frac{\sin \tilde{\omega}}{\tilde{\omega}} \right) \mathcal{S}_{jk} - \frac{\cos \tilde{\omega}}{\tilde{\omega}} \right] \right\}. \quad (46)$$

For marginals (i.e., when $j = k$), the expression reduces to the known formula for PSD of 1-dimensional fBm with Hurst parameter $H = H_j = H_k$ ¹⁶, since $\eta_{jj} = 0$. In contrast, for $j \neq k$, the cross power spectral density acquires an imaginary part in the causal case, reflecting time-asymmetric dependence between components. This imaginary component vanishes in the well-balanced case, where $\eta_{jk} \equiv 0$ (cf. Eq. (16)).

Theorem 5 (Asymptotic behavior of the ensemble-averaged PSD). *The ensemble-averaged PSD $\langle S_{jk}(\tilde{\omega}, T) \rangle$ of the 2D fBm admits the following asymptotic regimes as $\tilde{\omega} \rightarrow \infty$ if $H_j +$*

$H_k \neq 1$ or for well-balanced 2D fBm

$$\Re\langle S_{jk}(\tilde{\omega}, T) \rangle \sim T^{H_j+H_k+1} \sigma_j \sigma_k \rho_{jk} \left\{ \left[\frac{1}{\tilde{\omega}^2} - \frac{(H_j + H_k) \sin \tilde{\omega}}{\tilde{\omega}^3} + O\left(\frac{1}{\tilde{\omega}^4}\right) \right] + a_{jk} \left[\frac{1}{\tilde{\omega}^{H_j+H_k+1}} - \frac{(H_j + H_k + \cos \tilde{\omega}) \cot\left(\frac{\pi}{2}(H_j + H_k)\right) + \sin \tilde{\omega}}{\tilde{\omega}^{H_j+H_k+2}} \right] \right\}, \quad (47)$$

$$\Im\langle S_{jk}(\tilde{\omega}, T) \rangle \sim T^{H_j+H_k+1} \sigma_j \sigma_k \eta_{jk} \left\{ \left[\frac{2}{\tilde{\omega}^2} - \frac{3 - \cos \tilde{\omega}}{\tilde{\omega}^3} + O\left(\frac{1}{\tilde{\omega}^4}\right) \right] - a_{jk} \left[\frac{\cot\left(\frac{\pi}{2}(H_j + H_k)\right)}{\tilde{\omega}^{H_j+H_k+1}} + \frac{2 + H_j + H_k - \cos \tilde{\omega} + \sin \tilde{\omega} \cot\left(\frac{\pi}{2}(H_j + H_k)\right)}{\tilde{\omega}^{H_j+H_k+2}} \right] \right\}, \quad (48)$$

where \Re and \Im denote the real and imaginary parts, respectively. Parameters ρ_{jk} and η_{jk} are given in [Theorem 1](#). In the formulas above, the parameters $a_{jk} = \Gamma(H_j + H_k) \sin\left(\frac{\pi}{2}(H_j + H_k)\right)$.

Proof. The proof of this theorem is based on the asymptotic expansion of the incomplete gamma function and is presented in details in [Appendix section F](#). \square

The behavior of ensemble-averaged PSD of 2D fBm depends explicitly on the Hurst parameters H_j , H_k , as well as the parameters ρ_{jk} and η_{jk} . In the following remark we present the details.

Remark 9. *The asymptotic behavior of the ensemble-averaged PSD $\langle S_{jk}(\tilde{\omega}, T) \rangle$ for 2D fBm depends on whether the sum of Hurst parameters $H_j + H_k$ is greater than or smaller than 1. In particular, when $H_j + H_k > 1$, we observe dependence on measurement time T . More precisely, we have*

$$\Re\langle S_{jk}(f, T) \rangle \sim \sigma_j \sigma_k \rho_{jk} \left[\frac{1}{f^2} T^{H_j+H_k-1} + \frac{a_{jk}}{f^{H_j+H_k+1}} + o(1) \right], \quad (49)$$

$$\Im\langle S_{jk}(f, T) \rangle \sim \sigma_j \sigma_k \eta_{jk} \left[\frac{2}{f^2} T^{H_j+H_k-1} - \frac{a_{jk} \cot\left(\frac{\pi}{2}(H_j + H_k)\right)}{f^{H_j+H_k+1}} + o(1) \right], \quad (50)$$

Conversely, for $H_j + H_k < 1$, the decay is faster, and the cross-component interactions diminish more rapidly with frequency

$$\Re\langle S_{jk}(f, T) \rangle \sim \sigma_j \sigma_k \rho_{jk} \left[\frac{a_{jk}}{f^{H_j+H_k+1}} + \frac{1}{f^2 T^{1-H_j-H_k}} + o\left(T^{H_j+H_k-1}\right) \right], \quad (51)$$

$$\Im\langle S_{jk}(f, T) \rangle \sim \sigma_j \sigma_k \eta_{jk} \left[\frac{-a_{jk} \cot\left(\frac{\pi}{2}(H_j + H_k)\right)}{f^{H_j+H_k+1}} + \frac{2}{f^2 T^{1-H_j-H_k}} + o\left(T^{H_j+H_k-1}\right) \right] \quad (52)$$

This dichotomy highlights the crucial role of $H_j + H_k$ on the spectral structure of the process.

V. NUMERICAL SIMULATIONS

In this section, we present the comparison of the analytical results obtained in the previous parts of this article with numerical simulations. For the numerical simulations of 2D fBm we apply the Wood and Chan's algorithm⁶⁶, which is based on embedding the covariance matrix of 2D fBm increments into a circulant matrix. All of the presented numerical results are based on the ensemble of $N = 5,000$ trajectories of length $T = 2^{16} = 65,536$ with a time step 1.

A. Trajectories

To visualize 2D fBm and evaluate our analytical results, we performed extensive numerical simulations. Figures 2 and 3 show sample trajectories of the 2D fBm. In both figures, upper row corresponds to the case of independent coordinates, i.e., $\rho = \rho_{12} = 0$, while the bottom row corresponds to the case $\rho_{12} = 0.5$. In Figure 2 we present the case with $H_1 = H_2$, that is, a case when causal and well-balanced processes coincide. In Figure 3 we focus on the case with $H_1 \neq H_2$ and the trajectories are realizations of the causal 2D fBm. We present more trajectories to highlight the difference in the behavior of the process in the cardinal directions. For example, on panels (b) and (d), the process is characterized by subdiffusion on the horizontal axis (1st coordinate) while on the vertical it is a superdiffusion (2nd coordinate).

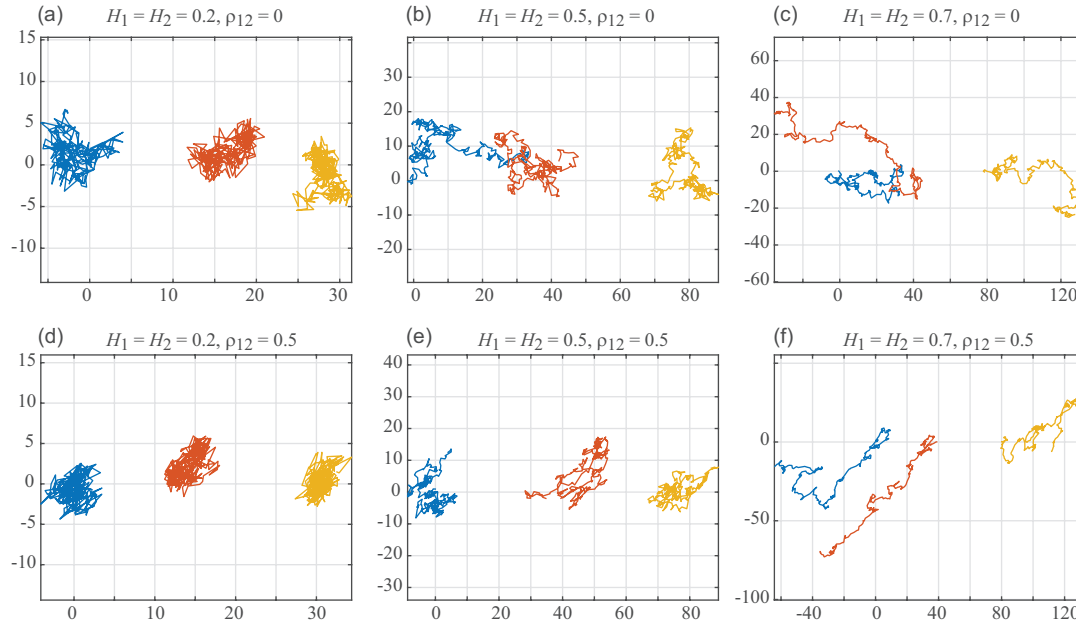


FIG. 2. Sample trajectories of causal 2D fBm with $H_1 = H_2 = H$. Each panel corresponds to a given set of parameters (H, ρ_{12}) , where the top row (a-c) corresponds to uncorrelated components and the bottom row (d-f) to cross-correlation $\rho_{12} = 0.5$. Pairs of panels in each column have the same H . The trajectories are shifted on the horizontal axis for clarity.

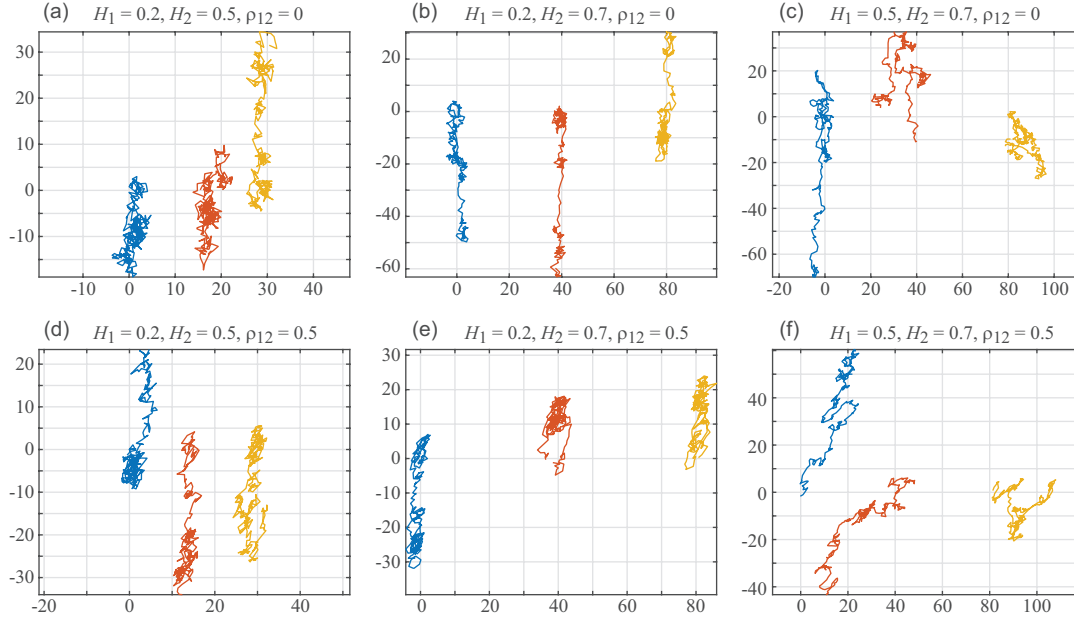


FIG. 3. Sample trajectories of causal 2D fBm with different Hurst exponents, $H_1 \neq H_2$. Each panel corresponds to a given set of parameters (H_1, H_2, ρ_{12}) , where the top row (a-c) corresponds to uncorrelated components and the bottom row (d-f) to cross-correlation $\rho_{12} = 0.5$. The trajectories are shifted on the horizontal axis for clarity.

B. Autocovariance

The different cases of cross-covariance functions γ_{12} given in [Theorem 1](#) are presented in [Figures 4 and 5](#). In both of these figures, the cross-covariance function for the causal version of the process is plotted using a solid line, while for well-balanced case, a dashed line is used. [Figure 4](#) showcases the situation when $H_1 = H_2$. However, as discussed in [Remark 3](#), in such a case both causal and well-balanced cases are the same – that is why the continuous and dashed lines overlap each other. We see that the cross-covariance function behaves similarly to that we expect for the fractional Brownian motion with the corresponding H . The only difference between cross-covariances of the causal and well-balanced processes is the rescaling of such function by a factor of ρ_{12} . Thus, each case (subdiffusive $H_1 = H_2 = 0.2$ – blue line, left panel; diffusive $H_1 = H_2 = 0.5$ – orange line, middle panel; superdiffusive $H_1 = H_2 = 0.7$ – yellow line, right panel) retains the behavior.

A more interesting situation is presented in [Figure 5](#), where the corresponding Hurst parameters H_1 and H_2 are not equal. Here, the dashed lines corresponding to the well-balanced case are different from the ones for causal 2D fBm. Particularly, it seems that the ‘strength’ of the cross-covariance is usually smaller (in the absolute sense) in such cases. The most interesting is the case of $H_1 = 0.2, H_2 = 0.7, \rho_{12} = 0.5$ (orange line, middle panel) – for which we change the type of memory for lags $h > 0$. For the causal case, the cross-covariance function was positive, while the addition of the well-balanced element makes it negative. Another interesting effect can be observed for the causal version for $H_1 = 0.2, H_2 = 0.5$ and $H_1 = 0.5, H_2 = 0.7$ and $\rho_{12} = 0.5$ in both cases. The cross-covariance function disappears

for $h > 0$ and $h < 0$, respectively. It is due to the fact that via the choice of parameters we obtained $\rho_{12} - \eta_{12}\text{sign}h = 0$ thus cancelling every element in the cross-covariance function for the increments for lags $|h| \geq 1$ (cf. the relation between ρ_{12} and η_{12} in Eq. (A22) of the Appendix).

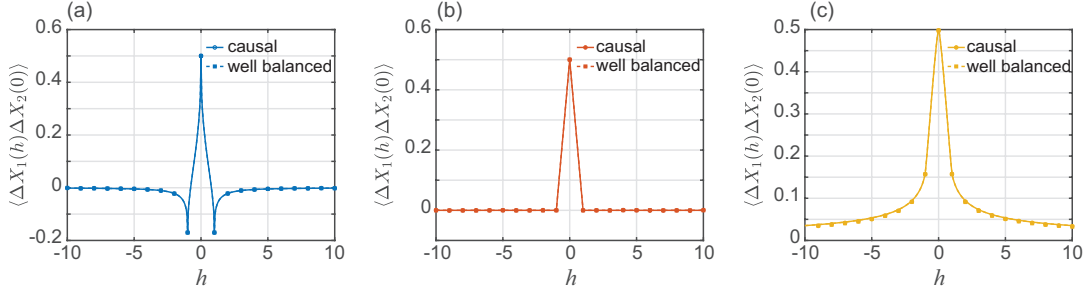


FIG. 4. Cross-covariance function depending on H_1, H_2 and $\rho_{12} = 0.5$ for $H_1 = H_2$. (a) $H_1 = H_2 = 0.2$, (b) $H_1 = H_2 = 0.5$, and (c) $H_1 = H_2 = 0.7$. The solid lines represent the causal version of the model and dashed lines the well-balanced case. Markers correspond to the estimated values of the cross-covariance function; circles correspond to the causal case, squares to the well-balanced case. Here, causal and well-balanced cases overlap, as for $H_1 = H_2$ the model is time-reversible regardless of the definition (cf. Eq. (15)). Increments are taken over a unit time interval, i.e., $\Delta \equiv \Delta^{\delta=1}$.

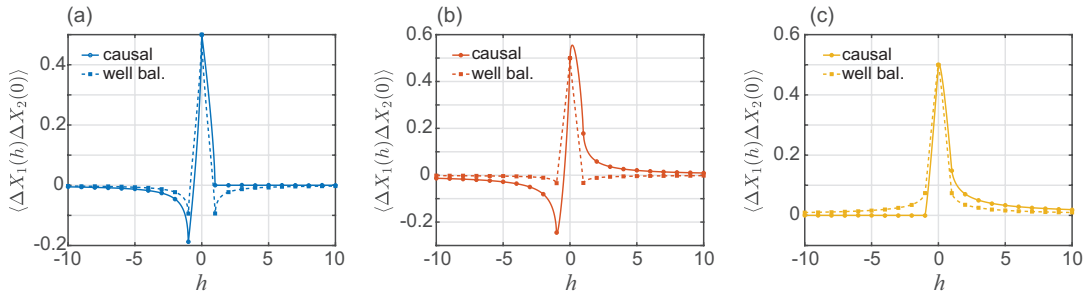


FIG. 5. Cross-covariance function depending on H_1, H_2 and ρ_{12} for $H_1 \neq H_2$. (a) $H_1 = 0.2, H_2 = 0.5$, (b) $H_1 = 0.2, H_2 = 0.7$, and (c) $H_1 = 0.5, H_2 = 0.7$. Solid lines represent the causal version of the model, the dashed lines the well-balanced case. Markers correspond to the estimated values of the cross-covariance function; circles correspond to the causal case, squares to the well-balanced case.

C. Spectral content

In Figure 6 we present a comparison between estimated ensemble-averaged (cross-)PSD to their theoretical asymptotics for the 2D fBm. As in previous figures, solid lines represent estimates from simulations, while dashed lines indicate the theoretical asymptotics. Different colored solid lines correspond to different sets of parameters (H_1, H_2) , whereas $\rho_{12} = 0.5$ for all the cases. Panels (a) and (b) present the real part, i.e., $\Re\langle S_{\mathbf{X},12}(f, T) \rangle$, with panel (a) corresponding to the case with $H_1 = H_2$ (i.e., when the causal and well-balanced 2D fBms coincide), while panel (b) represents the causal 2D fBm with $H_1 \neq H_2$. Panel (c) showcases the imaginary part, i.e., $\Im\langle S_{\mathbf{X},12}(f, T) \rangle$ for the sets $H_1 \neq H_2$ corresponding to panel (b) (as

for the $H_1 = H_2$ case, the cross-PSD is 0).

In all panels, we see that the asymptotic behavior of the ensemble-averaged cross-PSD depends on the $H_1 + H_2$ value: if it is smaller than 1, the asymptotic decay behaves like $f^{-1-H_1-H_2}$ (for large f), whereas if $H_1 + H_2 \geq 1$, then the asymptotic decay is proportional to f^{-2} .

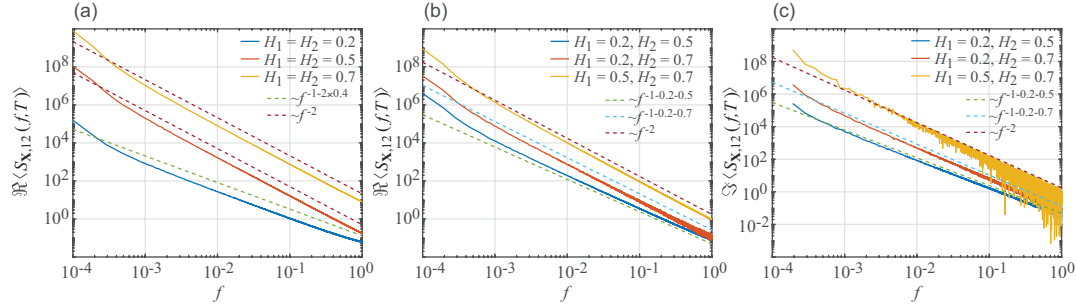


FIG. 6. Ensemble-averaged (cross-)PSD. Solid lines correspond to PSD estimated from the simulated trajectories, dashed lines to their asymptotics. (a) $\Re\langle S_{\mathbf{X},12}(f,T) \rangle$, $H_1 = H_2$; (b) $\Re\langle S_{\mathbf{X},12}(f,T) \rangle$, $H_1 \neq H_2$; and (c) $\Im\langle S_{\mathbf{X},12}(f,T) \rangle$, $H_1 \neq H_2$. In each case, $\rho_{12} = 0.5$. Since the real part for both causal and well-balanced case is the same, we plot only one corresponding line to each set of parameters. Conversely, the imaginary part for the well-balanced case is 0, so we plot only $\Im\langle S_{\mathbf{X},12} \rangle$ for the causal 2D fBm. In all the panels, $T = 2^{16} = 65,536$ and the lines are based on $N = 5,000$ trajectories.

Similarly to Figure 6, in Figure 7 we present a comparison between estimated ensemble-averaged (cross-)PSD to their theoretical asymptotics for the increments of 2D fBm. Again, solid lines represent estimates from simulations, while dashed lines indicate the theoretical asymptotics. Different colored solid lines correspond to different sets of parameters (H_1, H_2) , whereas $\rho_{12} = 0.5$ for all the cases. Panels (a) and (b) present the real part, i.e., $\Re\langle S_{\Delta\mathbf{X},12}(f,T) \rangle$, with panel (a) corresponding to the case with $H_1 = H_2$ (i.e., when the causal and well-balanced 2D fBms coincide), while panel (b) represents the causal 2D fBm increments with $H_1 \neq H_2$. Panel (c) showcases the imaginary part, i.e., $\Im\langle S_{\Delta\mathbf{X},12}(f,T) \rangle$ for the sets $H_1 \neq H_2$ corresponding to panel (b) (as for the $H_1 = H_2$ case, the cross-PSD is 0). In all panels, we see that the asymptotic behavior of the ensemble-averaged (cross-)PSD for increments behaves in a similar way in all cases, regardless if $H_1 + H_2 \geq 1$. The asymptotic behavior, as $f \rightarrow 0$ is proportional to $f^{1-H_1-H_2}$. Here, we see a quantitative difference of diverging or converging (cross-)PSD around 0 – if $H_1 + H_2 > 1$ then the (cross-)PSD diverges (in 1D, it corresponds to one of the definitions of long memory⁵²), while for $H_1 + H_2 < 1$ the (cross-)PSD converges to 0.

VI. CONCLUSIONS

In this work, we introduced a natural construction of 2D fBm that accounts for anisotropic scaling and cross-dimensional dependencies, extending the classical framework of Mandelbrot and van Ness to multivariate settings. By incorporating correlated Gaussian noises and a matrix-valued Hurst operator, we provided two distinct formulations, causal and well-balanced 2D fBm, and derived their respective auto- and cross-covariance across the two components. Our analysis highlights key differences between these two formulations, partic-

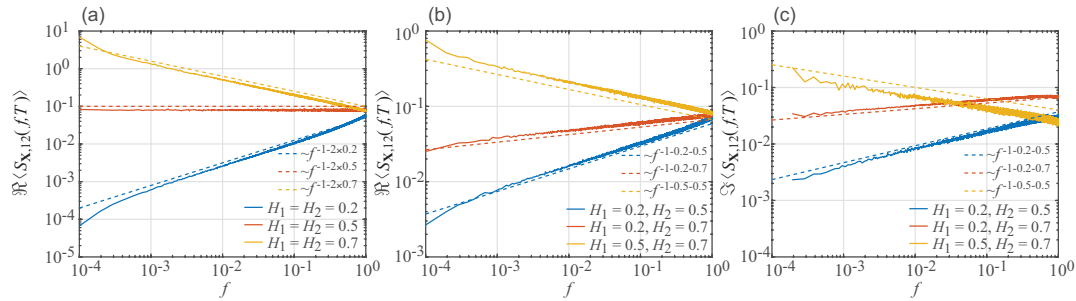


FIG. 7. Ensemble-averaged (cross-)PSD for increments. Continuous lines correspond to PSD estimated from the simulated trajectories' increments, dashed lines to their asymptotics. (a) $\Re\langle S_{12}^{\Delta}(f, T) \rangle$, $H_1 = H_2$; (b) $\Re\langle S_{12}^{\Delta}(f) \rangle$, $H_1 \neq H_2$; and (c) $\Im\langle S_{12}^{\Delta}(f) \rangle$, $H_1 \neq H_2$. In each case, $\rho_{12} = 0.5$. Since the real part for both causal and well-balanced case is the same, we plot only one corresponding line to each set of parameters. Conversely, the imaginary part for the well-balanced case is 0, so we plot only $\Im\langle S_{12}^{\Delta}(f) \rangle$ for the causal 2D fBm's increments. In all the panels, $T = 2^{16} = 65,536$ and the lines are based on $N = 5,000$ trajectories.

ularly in the asymmetry of causal fBm and implications for time-reversal. Furthermore, we analyzed the spectral properties of the processes, presenting both full analytical derivations and asymptotic behaviors in the frequency domain. Our results reveal how variations in the Hurst exponents and correlation structure manifest in the spectral content, offering new insights into the interpretation of multivariate time series in diverse systems. The results also clarify the qualitative distinction between the causal and well-balanced versions of the 2D fBm. While both share the same marginal scaling properties and stationary increments, their dependence structures differ substantially when $H_1 \neq H_2$. The causal model exhibits asymmetric cross-covariance structure and a phase shift in the spectral domain. In contrast, the well-balanced construction remains time-reversible for all parameter values, with symmetric cross-covariance and no cross-PSD structure. In this sense, the two formulations are complementary. The difference between the models provides a means to identify a model in a real data set. A notable case arises when $H_1 = H_2$. In this situation, the process remains a 2D fBm under arbitrary rotations. In contrast, when $H_1 \neq H_2$, a rotation mixes the coordinates in such a way that the resulting marginals are no longer fBm, but instead they exhibit more complex dependencies. A 2D processes with $H_1 = H_2$ can thus describe a system with two-component fBm in the same geometric space, such as the two-dimensional motion of particles in a complex environment with underlying non-uniform structure. On the other hand, $H_1 \neq H_2$ describes a more general case where each component may represent a different fBm, albeit exhibiting correlations. Such two-component processes can emerge in diverse systems. To name a few examples: in climate science, they can describe temperature^{67,68} and precipitation¹⁰; in hydrology, river flows^{10,69} and erosion⁷⁰; and in physiology, heart rate⁷¹ and breathing patterns⁷².

Extensive numerical simulations validated our theoretical findings, demonstrating consistency in both the time and frequency domains. The proposed framework thus provides a robust tool for modeling and analyzing complex anomalous diffusion processes in multidimensional environments, especially in settings where directional dependence and inter-component correlations cannot be ignored. This study opens several avenues for further exploration. A potential immediate extension involves generalizing the proposed constructions and results

to higher dimensions. Our work opens the way to the application of 2D fBm to empirical data in fields such as neuroscience, single-particle tracking, structural dynamics, and financial econometrics, which may yield new insights into underlying spatiotemporal correlations.

ACKNOWLEDGEMENTS

This work was supported by NCN OPUS project No. 2024/53/B/HS4/00433 (to AW) and by the National Science Foundation (NSF) Grant 2102832 (to DK).

Appendix A: Proof of [Theorem 1](#), causal case and some additional remarks

Proof. Comparing the definition of the proposed causal 2D fBm process (cf. [Definition 1](#)) to the definition of operator fractional Brownian motion $B_H(t), t \geq 0$, given in formula (9.3.22) from⁵²,

$$B_H(t) = \int_{\mathbb{R}} ((t-u)_+^D - (-u)_+^D) M_+ + ((t-u)_-^D - (-u)_-^D) M_- B(du), \quad (\text{A1})$$

we see that for our causal 2D fBm is equivalent when the matrices M_+ and M_- are as follows

$$M_+ = \begin{bmatrix} \sigma_1 a_{H_1} & 0 \\ \rho \sigma_2 a_{H_2} & \sqrt{1 - \rho^2} \sigma_2 a_{H_2} \end{bmatrix}, \quad (\text{A2})$$

$$M_- = 0 \cdot I_2, \quad (\text{A3})$$

for a size-two identity matrix I_2 .

Utilizing (9.3.28-29) from⁵²i.e.,

$$M_+ - M_- = \sqrt{2\pi} \left[\sin \left(\frac{D\pi}{2} \right) \right]^{-1} \Gamma(D+I)^{-1} A_1, \quad (\text{A4})$$

$$M_+ + M_- = \sqrt{2\pi} \left[\sin \left(\frac{D\pi}{2} \right) \right]^{-1} \Gamma(D+I)^{-1} A_2, \quad (\text{A5})$$

we can calculate $A = A_1 + iA_2$ that later will be used for determining the covariance structure of the proposed process

$$A_1 = \frac{1}{\sqrt{2\pi}} \Gamma(D+I) \cdot \sin \left(\frac{D\pi}{2} \right) M_+, \quad (\text{A6})$$

$$A_2 = \frac{1}{\sqrt{2\pi}} \Gamma(D+I) \cdot \cos \left(\frac{D\pi}{2} \right) M_+, \quad (\text{A7})$$

where $D = H - \frac{1}{2}I$ is a 2x2 matrix, and all of the present functions (Γ , \sin , \cos) are understood as the primary matrix functions (def. 9.3.4 in⁵²). Therefore, we can explicitly write

$$\begin{aligned} A_1 &= \frac{1}{\sqrt{2\pi}} \begin{bmatrix} \Gamma(H_1 + \frac{1}{2}) & 0 \\ 0 & \Gamma(H_2 + \frac{1}{2}) \end{bmatrix} \cdot \begin{bmatrix} \sin \left(\frac{(H_1 - \frac{1}{2})\pi}{2} \right) & 0 \\ 0 & \sin \left(\frac{(H_2 - \frac{1}{2})\pi}{2} \right) \end{bmatrix} \cdot \begin{bmatrix} \sigma_1 a_{H_1} & 0 \\ \rho \sigma_2 a_{H_2} & \sqrt{1 - \rho^2} \sigma_2 a_{H_2} \end{bmatrix} \\ &= \begin{bmatrix} \Gamma(H_1 + \frac{1}{2}) \sin \left(\frac{(H_1 - \frac{1}{2})\pi}{2} \right) \sigma_1 a_{H_1} & 0 \\ \rho \Gamma(H_2 + \frac{1}{2}) \sin \left(\frac{(H_2 - \frac{1}{2})\pi}{2} \right) \sigma_2 a_{H_2} & \sqrt{1 - \rho^2} \Gamma(H_2 + \frac{1}{2}) \sin \left(\frac{(H_2 - \frac{1}{2})\pi}{2} \right) \sigma_2 a_{H_2} \end{bmatrix}, \quad (\text{A8}) \end{aligned}$$

and similarly for A_2

$$A_2 = \frac{1}{\sqrt{2\pi}} \begin{bmatrix} \Gamma(H_1 + \frac{1}{2}) \cos\left(\frac{(H_1 - \frac{1}{2})\pi}{2}\right) \sigma_1 a_{H_1} & 0 \\ \rho \Gamma(H_2 + \frac{1}{2}) \cos\left(\frac{(H_2 - \frac{1}{2})\pi}{2}\right) \sigma_2 a_{H_2} & \sqrt{1 - \rho^2} \Gamma(H_2 + \frac{1}{2}) \cos\left(\frac{(H_2 - \frac{1}{2})\pi}{2}\right) \sigma_2 a_{H_2} \end{bmatrix}. \quad (\text{A9})$$

Thus, $A = A_1 + iA_2$ can be written as

$$A = \frac{1}{\sqrt{2\pi}} \begin{bmatrix} \Gamma(H_1 + \frac{1}{2}) \exp\{i\frac{\pi}{2}(\frac{3}{2} - H_1)\} \sigma_1 a_{H_1} & 0 \\ \rho \Gamma(H_2 + \frac{1}{2}) \exp\{i\frac{\pi}{2}(\frac{3}{2} - H_2)\} \sigma_2 a_{H_2} & \sqrt{1 - \rho^2} \Gamma(H_2 + \frac{1}{2}) \exp\{i\frac{\pi}{2}(\frac{3}{2} - H_2)\} \sigma_2 a_{H_2} \end{bmatrix}. \quad (\text{A10})$$

In order to obtain the covariance structure, we calculate $C = [c_{jk}]_{j,k=1,2} = AA^*$ (from Proposition 9.3.19⁵²). In our case, its elements are given by

$$\begin{cases} c_{jj} &= \frac{1}{2\pi} \sigma_j^2 \Gamma^2(H_j + 0.5) a_{H_j}^2, \\ c_{jk} &= \frac{1}{2\pi} \rho \sigma_j \sigma_k \Gamma(H_j + 0.5) \Gamma(H_k + 0.5) a_{H_j} a_{H_k} e^{-i\frac{\pi}{2}(H_j - H_k)}, \quad j \neq k, \end{cases} \quad (\text{A11})$$

for $j, k = 1, 2$. Note that the matrix C is Hermitian, $C = C^*$, and thus its diagonal elements are real. According to Proposition 9.3.19⁵², the covariance structure is

$$\gamma_{jk}(t, s) \equiv \langle X_j(t) X_k(s) \rangle = \frac{\sigma_j \sigma_k}{2} (w_{jk}(t) |t|^{H_j + H_k} + w_{jk}(-s) |s|^{H_j + H_k} - w_{jk}(t - s) |t - s|^{H_j + H_k}), \quad (\text{A12})$$

where $\sigma_j^2 = \langle X_j^2(1) \rangle$ and

$$w_{jk}(u) = \begin{cases} \rho_{jk} - \eta_{jk} \text{sign}(u), & H_j + H_k \neq 1, \\ \rho_{jk} - \eta_{jk} \text{sign}(u) \log |u|, & H_j + H_k = 1. \end{cases} \quad (\text{A13})$$

□

The connection between the elements of matrix C given in Eq. (A11) and the parameters ρ_{jk} and η_{jk} are as follows

$$\sigma_j \sigma_k \rho_{jk} = 4b_1 \left(\frac{H_j + H_k}{2} \right) \Re(c_{jk}), \quad (\text{A14})$$

$$\sigma_j \sigma_k \eta_{jk} = 4b_2 \left(\frac{H_j + H_k}{2} \right) \Im(c_{jk}), \quad (\text{A15})$$

where

$$b_1(H) = \begin{cases} \frac{\Gamma(2-2H) \cos(H\pi)}{2H(1-2H)}, & H \neq \frac{1}{2}, \\ \frac{\pi}{2}, & H = \frac{1}{2}, \end{cases} \quad (\text{A16})$$

$$b_2(H) = \frac{\Gamma(2-2H) \sin(H\pi)}{2H(1-2H)}. \quad (\text{A17})$$

Let us calculate ρ_{jk} explicitly. First, consider $j = k$, and assume that $H_j \neq \frac{1}{2}$. We have

$$\begin{aligned}
\sigma_j \sigma_j \rho_{jj} &= 4b_1 \left(\frac{H_j + H_j}{2} \right) \Re(c_{jj}) = 4b_1(H_j) \Re(c_{jj}) \\
&= 4 \frac{\Gamma(2 - 2H_j) \cos(H_j \pi)}{2H_j(1 - 2H_j)} \frac{1}{2\pi} \Gamma^2 \left(H_j + \frac{1}{2} \right) \sigma_j^2 a_{H_j}^2 \\
&\quad \Gamma(z) \Gamma(1-z) = \frac{\pi}{\sin(\pi z)} \\
&= 4\sigma_j^2 \frac{\overbrace{\Gamma(1 - 2H_j)}^{\Gamma(z) \Gamma(1-z) = \frac{\pi}{\sin(\pi z)}} \cos(H_j \pi)}{2H_j} \frac{1}{2\pi} \Gamma^2 \left(H_j + \frac{1}{2} \right) a_{H_j}^2 \\
&= 2\sigma_j^2 \frac{\cos(H_j \pi)}{\underbrace{2H_j \Gamma(2H_j)}_{\Gamma(2H_j+1)} \sin(2H_j \pi)} \Gamma^2 \left(H_j + \frac{1}{2} \right) \underbrace{a_{H_j}^2}_{= \frac{\Gamma(2H_j+1) \sin(H_j \pi)}{\Gamma^2(H_j + \frac{1}{2})}} \\
&= \sigma_j^2. \tag{A18}
\end{aligned}$$

Therefore, $\rho_{jj} = 1$ as expected from the correlation coefficient between $X_j(1)$ and $X_j(1)$.

Now, let us deal with the more interesting case, i.e., ρ_{12} . We have the following

$$\begin{aligned}
\sigma_1 \sigma_2 \rho_{12} &= 4b_1 \left(\frac{H_1 + H_2}{2} \right) \Re(c_{12}) \\
&= 4 \frac{\Gamma(2 - (H_1 + H_2)) \cos\left(\frac{H_1 + H_2}{2} \pi\right)}{(H_1 + H_2)(1 - (H_1 + H_2))} \frac{1}{2\pi} \Gamma \left(H_1 + \frac{1}{2} \right) \Gamma \left(H_2 + \frac{1}{2} \right) \rho \sigma_1 \sigma_2 a_{H_1} a_{H_2} \cos \left(\frac{(H_2 - H_1)\pi}{2} \right) \\
&\quad \Gamma(z) \Gamma(1-z) = \frac{\pi}{\sin(\pi z)} \\
&= 4\rho \sigma_1 \sigma_2 \frac{\overbrace{\Gamma(1 - (H_1 + H_2))}^{\Gamma(z) \Gamma(1-z) = \frac{\pi}{\sin(\pi z)}} \cos\left(\frac{H_1 + H_2}{2} \pi\right)}{H_1 + H_2} \frac{1}{2\pi} \Gamma \left(H_1 + \frac{1}{2} \right) \Gamma \left(H_2 + \frac{1}{2} \right) a_{H_1} a_{H_2} \cos \left(\frac{(H_2 - H_1)\pi}{2} \right) \\
&= 2\rho \sigma_1 \sigma_2 \frac{\pi}{\sin((H_1 + H_2)\pi) \Gamma(H_1 + H_2)} \frac{\cos\left(\frac{H_1 + H_2}{2} \pi\right)}{H_1 + H_2} \frac{1}{\pi} \Gamma \left(H_1 + \frac{1}{2} \right) \Gamma \left(H_2 + \frac{1}{2} \right) \underbrace{a_{H_1}}_{= \frac{\sqrt{\Gamma(2H_1+1) \sin(H_1 \pi)}}{\Gamma(H_1 + \frac{1}{2})}} a_{H_2} \cos \left(\frac{(H_2 - H_1)\pi}{2} \right) \\
&= \rho \sigma_1 \sigma_2 \frac{\sqrt{\Gamma(2H_1 + 1) \Gamma(2H_2 + 1) \sin(H_1 \pi) \sin(H_2 \pi)}}{\Gamma(H_1 + H_2 + 1) \sin\left(\frac{H_1 + H_2}{2} \pi\right)} \cos \left(\frac{(H_2 - H_1)\pi}{2} \right). \tag{A19}
\end{aligned}$$

Thus, the cross-correlation ρ_{12} is given by

$$\rho_{12} = \rho \frac{\sqrt{\Gamma(2H_1 + 1) \Gamma(2H_2 + 1) \sin(H_1 \pi) \sin(H_2 \pi)}}{\Gamma(H_1 + H_2 + 1) \sin\left(\frac{H_1 + H_2}{2} \pi\right)} \cos \left(\frac{(H_2 - H_1)\pi}{2} \right). \tag{A20}$$

Note that, for the special case $H_1 = H_2$, the cross-correlation ρ_{12} is equal to the correlation between noises, i.e., $\rho_{12} = \rho$. Lastly, to have the full covariance structure, we need to calculate coefficients η_{jk} . First, as $\Im(c_{jj}) = 0$ (C being a Hermitian matrix), we have $\eta_{jj} = 0$ for $j = 1, 2$. The more interesting case is $j \neq k$, which after similar calculations as for ρ_{12} leads to

$$\eta_{12} = \rho \frac{\sqrt{\Gamma(2H_1 + 1) \Gamma(2H_2 + 1) \sin(H_1 \pi) \sin(H_2 \pi)}}{\Gamma(H_1 + H_2 + 1) \cos\left(\frac{H_1 + H_2}{2} \pi\right)} \sin \left(\frac{(H_2 - H_1)\pi}{2} \right). \tag{A21}$$

It can be expressed as

$$\eta_{12} = \rho_{12} \tan \left(\pi \frac{H_2 - H_1}{2} \right) \tan \left(\pi \frac{H_1 + H_2}{2} \right) = -\rho_{12} \tan \left(\pi \frac{H_1 - H_2}{2} \right) \tan \left(\pi \frac{H_1 + H_2}{2} \right), \tag{A22}$$

which coincides with the results for the causal process given in Section 3.3 of¹⁴.

Appendix B: Construction of a well-balanced 2D fBm

First, let us consider a one-dimensional well-balanced fractional Brownian motion given in Definition 3 below.

Definition 3 (Well-balanced 1D fBm). *Well-balanced fractional Brownian motion $X^*(t), t \geq 0$, is given by the following time-domain representation*

$$X^*(t) = a_H^* \int_{\mathbb{R}} \left((t-u)_+^{H-\frac{1}{2}} - (-u)_+^{H-\frac{1}{2}} \right) + \left((t-u)_-^{H-\frac{1}{2}} - (-u)_-^{H-\frac{1}{2}} \right) B(du), \quad (\text{B1})$$

where $H \in (0, 1)$ and $a_H^* > 0$.

Theorem 6. *The constant a_H^* for which $\langle X^{*2}(t) \rangle = 1$ for the well-balanced 1D fBm is given by*

$$a_H^{*2} = \frac{2H(1-2H)\pi}{8\Gamma(2-2H)\cos(H\pi)\Gamma^2(H+\frac{1}{2})\cos^2\left(\frac{\pi(H-\frac{1}{2})}{2}\right)}.$$

Proof. Let us recall the definition of the function given in Eq. (1)

$$f_{\pm}(x; t, \beta) = (t-x)_{\pm}^{\beta} - (-x)_{\pm}^{\beta}.$$

In order to calculate the autocovariance of the process, let us first utilize Itô's lemma. We have

$$\begin{aligned} \langle X^*(t)X^*(s) \rangle &= a_H^{*2} \int_{\mathbb{R}} (f_+(u; t, D) + f_-(u; t, D))(f_+(u; s, D) + f_-(u; s, D)) du \\ &\stackrel{\text{Plancherel}}{=} \frac{a_H^{*2}}{2\pi} \int_{\mathbb{R}} (\widehat{f}_+(\xi; t, D) + \widehat{f}_-(\xi; t, D)) \overline{(\widehat{f}_+(\xi; s, D) + \widehat{f}_-(\xi; s, D))} d\xi, \end{aligned} \quad (\text{B2})$$

where \bar{z} is a complex conjugate of z and $\widehat{f}_{\pm}(\xi; t, D)$ is a Fourier transform of f_{\pm} . Thus, it is given by⁷³ (formulae 3.76.4 and 3.76.9)

$$\widehat{f}_{\pm}(\xi; t, D) \equiv \int_{\mathbb{R}} e^{i u \xi} f(u; t, D) du = \frac{e^{it\xi} - 1}{ix|x|^D} \Gamma(D+1) e^{\mp i \text{sign}(x) \frac{\pi D}{2}} \quad (\text{B3})$$

and

$$\widehat{f}_+(\xi; t, D) + \widehat{f}_-(\xi; t, D) = \frac{e^{it\xi} - 1}{ix|x|^D} \Gamma(D+1) 2 \cos^2\left(\frac{\pi D}{2}\right). \quad (\text{B4})$$

Consequently, the autocovariance function becomes

$$\begin{aligned} \langle X^*(t)X^*(s) \rangle &= \frac{a_H^{*2}}{2\pi} \int_{\mathbb{R}} \frac{e^{itx} - 1}{ix|x|^D} \frac{e^{-isx} - 1}{-ix|x|^D} \Gamma^2(D+1) 4 \cos^2\left(\frac{\pi D}{2}\right) dx = \\ &= 4 \frac{a_H^{*2}}{2\pi} \Gamma^2(D+1) \cos^2\left(\frac{\pi D}{2}\right) \int_{\mathbb{R}} \frac{(e^{itx} - 1)(e^{-isx} - 1)}{|x|^{2(D+1)}} dx. \end{aligned} \quad (\text{B5})$$

When $t = s = 1$ we have

$$\begin{aligned} \langle X^{*2}(1) \rangle &= 4 \frac{a_H^{*2}}{2\pi} \Gamma^2(D+1) \cos^2\left(\frac{\pi D}{2}\right) \int_{\mathbb{R}} \frac{(e^{ix} - 1)(e^{-ix} - 1)}{|x|^{2(D+1)}} dx \\ &= \frac{4a_H^{*2}}{\pi} \Gamma^2(D+1) \cos^2\left(\frac{\pi D}{2}\right) \int_{\mathbb{R}} \frac{1 - \cos x}{|x|^{2(D+1)}} dx \\ &= \frac{a_H^{*2}}{\pi} \Gamma^2(D+1) \cos^2\left(\frac{\pi D}{2}\right) \frac{4\pi}{\Gamma(2(D+1)) \sin((D+\frac{1}{2})\pi)} \\ &= \frac{a_H^{*2}}{\pi} \Gamma^2\left(H+\frac{1}{2}\right) \cos^2\left(\frac{\pi(H-\frac{1}{2})}{2}\right) \frac{4\pi}{\Gamma(2H+1) \sin(H\pi)}. \end{aligned} \quad (\text{B6})$$

To ensure that the variance of the process $X^*(t)$ is equal to 1 at time $t = 1$, the constant a_H has to be as follows

$$\begin{aligned} a_H^{*2} &= \frac{2H\Gamma(2H) \sin(\pi H)}{4\Gamma^2(H + \frac{1}{2}) \cos^2\left(\frac{\pi(H-\frac{1}{2})}{2}\right)} \\ &= \frac{2H(1-2H)\pi}{8\Gamma(2-2H) \cos(H\pi)\Gamma^2(H + \frac{1}{2}) \cos^2\left(\frac{\pi(H-\frac{1}{2})}{2}\right)}. \end{aligned} \quad (\text{B7})$$

□

Appendix C: Proof of [Theorem 1](#), well-balanced case and remarks

Proof. Again, looking at the general form given in Eq. [\(A1\)](#), we can calculate matrices M_+ , M_- and then, A_1 , A_2 and C . It is clear that matrices M_+ and M_- are the same, and given by

$$M_{\pm} = \begin{bmatrix} a_{H_1}^* \sigma_1 & 0 \\ a_{H_2}^* \rho \sigma_2 & a_{H_2}^* \sqrt{1-\rho^2} \sigma_2 \end{bmatrix}. \quad (\text{C1})$$

Thus, by the relations given in Eqs. [\(A4\)](#)-[\(A5\)](#) we have

$$A_1 = 0 \cdot I, \quad (\text{C2})$$

$$A_2 = \sqrt{\frac{2}{\pi}} \cos \frac{D\pi}{2} \Gamma(D+I) M_+ = \begin{bmatrix} a_{H_1}^* \sigma_1 \cos\left(\frac{(H_1-\frac{1}{2})\pi}{2}\right) \Gamma(H_1 + \frac{1}{2}) & 0 \\ a_{H_2}^* \rho \sigma_2 \cos\left(\frac{(H_2-\frac{1}{2})\pi}{2}\right) \Gamma(H_2 + \frac{1}{2}) & a_{H_2}^* \sqrt{1-\rho^2} \sigma_2 \cos\left(\frac{(H_2-\frac{1}{2})\pi}{2}\right) \Gamma(H_2 + \frac{1}{2}) \end{bmatrix}. \quad (\text{C3})$$

In the case of well-balanced 2D fBm, $A = A_1 + iA_2$ can be written as

$$A = iA_2 = i \begin{bmatrix} a_{H_1}^* \sigma_1 \cos\left(\frac{(H_1-\frac{1}{2})\pi}{2}\right) \Gamma(H_1 + \frac{1}{2}) & 0 \\ a_{H_2}^* \rho \sigma_2 \cos\left(\frac{(H_2-\frac{1}{2})\pi}{2}\right) \Gamma(H_2 + \frac{1}{2}) & a_{H_2}^* \sqrt{1-\rho^2} \sigma_2 \cos\left(\frac{(H_2-\frac{1}{2})\pi}{2}\right) \Gamma(H_2 + \frac{1}{2}) \end{bmatrix}. \quad (\text{C4})$$

Since $A = A_1 + iA_2 = iA_2$ and $C = AA^*$, elements of C are given by

$$\begin{cases} c_{jj} &= \frac{2}{\pi} \sigma_j^2 \cos^2\left(\frac{(H_j-0.5)\pi}{2}\right) \Gamma^2(H_j + 0.5) a_{H_j}^{*2}, \\ c_{jk} &= \frac{2}{\pi} \rho \sigma_j \sigma_k \cos\left(\frac{(H_j-0.5)\pi}{2}\right) \cos\left(\frac{(H_k-0.5)\pi}{2}\right) \Gamma(H_j + 0.5) \Gamma(H_k + 0.5) a_{H_j}^* a_{H_k}^*, \quad j \neq k, \end{cases} \quad (\text{C5})$$

for $j, k = 1, 2$. We note that C is a real matrix, in contrast to its equivalent in the causal 2D fBm. The consequence of that is that $\eta_{jk} = 0$ for all $j, k = 1, 2$, and therefore this is a time-reversible version of a 2D fBm. Thus, the covariance structure of two-dimensional well-balanced 2D fBm simplifies to

$$\langle X_j^*(t) X_k^*(s) \rangle = \frac{\sigma_j \sigma_k \rho_{jk}}{2} (|t|^{H_j+H_k} + |s|^{H_j+H_k} - |t-s|^{H_j+H_k}). \quad (\text{C6})$$

□

We can also calculate coefficients ρ_{jk} present in the covariance structure

$$\begin{aligned} \sigma_j^2 \rho_{jj} &= 4b_1(H_j) \Re(c_{jj}) = 4 \underbrace{\frac{\Gamma(2-2H_j) \cos(H_j \pi)}{2H_j(1-2H_j)}}_{b_1(H_j)} \underbrace{\frac{2}{\pi} \sigma_j^2 a_{H_j}^2 \Gamma^2 \left(H_j + \frac{1}{2} \right) \cos^2 \left(\frac{(H_j - \frac{1}{2})\pi}{2} \right)}_{c_{jj}} \\ &= 4 \frac{\Gamma(2-2H_j) \cos(H_j \pi)}{2H_j(1-2H_j)} \frac{2}{\pi} \sigma_j^2 \Gamma \left(H_j + \frac{1}{2} \right) \cos^2 \left(\frac{(H_j - \frac{1}{2})\pi}{2} \right) \frac{2H_j(1-2H_j)\pi}{8\Gamma(2-2H_j) \cos(\pi H_j) \Gamma^2 \left(H_j + \frac{1}{2} \right) \cos^2 \left(\frac{(H_j - \frac{1}{2})\pi}{2} \right)} = \sigma_j^2. \end{aligned} \quad (C7)$$

As expected $\rho_{jj} = 1$, since it is a correlation of $X_j^*(1)$ with itself. For more interesting case, i.e., for ρ_{12} , we have

$$\begin{aligned} \sigma_1 \sigma_2 \rho_{12} &= 4b_1 \left(\frac{H_1 + H_2}{2} \right) \Re(c_{12}) = \\ &= 4 \underbrace{\frac{\Gamma(2 - (H_1 + H_2)) \cos \left(\frac{(H_1 + H_2)\pi}{2} \right)}{(H_1 + H_2)(1 - (H_1 + H_2))}}_{b_1 \left(\frac{H_1 + H_2}{2} \right)} \underbrace{\frac{2}{\pi} \cos \left(\frac{(H_1 - \frac{1}{2})\pi}{2} \right) \Gamma \left(H_1 + \frac{1}{2} \right) \cos \left(\frac{(H_2 - \frac{1}{2})\pi}{2} \right) \Gamma \left(H_2 + \frac{1}{2} \right)}_{\Re(c_{12})} \sigma_1 \sigma_2 a_{H_1}^* a_{H_2}^* \rho \\ &= \frac{8}{\pi} \sigma_1 \sigma_2 \rho \frac{\Gamma(2 - (H_1 + H_2)) \cos \left(\frac{(H_1 + H_2)\pi}{2} \right)}{(H_1 + H_2)(1 - (H_1 + H_2))} \frac{\cos \left(\frac{(H_1 - \frac{1}{2})\pi}{2} \right) \Gamma \left(H_1 + \frac{1}{2} \right) \cos \left(\frac{(H_2 - \frac{1}{2})\pi}{2} \right) \Gamma \left(H_2 + \frac{1}{2} \right) \sqrt{2H_1(1-2H_1)} \sqrt{2H_2(1-2H_2)} \pi}{8\sqrt{\Gamma(2-2H_1) \cos(\pi H_1)} \sqrt{\Gamma(2-2H_2) \cos(\pi H_2)} \Gamma \left(H_1 + \frac{1}{2} \right) \cos \left(\frac{(H_1 - \frac{1}{2})\pi}{2} \right) \Gamma \left(H_2 + \frac{1}{2} \right) \cos \left(\frac{(H_2 - \frac{1}{2})\pi}{2} \right)} \\ &= \sigma_1 \sigma_2 \rho \frac{\cos \left(\frac{(H_1 + H_2)\pi}{2} \right)}{\Gamma(H_1 + H_2 + 1) \sin((H_1 + H_2)\pi)} \frac{\sqrt{\Gamma(2H_1 + 1) \Gamma(2H_2 + 1) \sin(2H_1\pi) \sin(2H_2\pi)}}{\sqrt{\cos(H_1\pi) \cos(H_2\pi)}} \\ &= \sigma_1 \sigma_2 \rho \frac{\sqrt{\Gamma(2H_1 + 1) \Gamma(2H_2 + 1)} \sqrt{\sin(H_1\pi) \sin(H_2\pi)}}{\Gamma(H_1 + H_2 + 1) \sin \left(\frac{(H_1 + H_2)\pi}{2} \right)}. \end{aligned} \quad (C8)$$

And thus,

$$\rho_{12} = \rho \frac{\sqrt{\Gamma(2H_1 + 1) \Gamma(2H_2 + 1)} \sqrt{\sin(H_1\pi) \sin(H_2\pi)}}{\Gamma(H_1 + H_2 + 1) \sin \left(\frac{(H_1 + H_2)\pi}{2} \right)}, \quad (C9)$$

which differs from the one given in the causal case missing a $\cos \left(\frac{(H_2 - H_1)\pi}{2} \right)$ factor. Similarly, the condition that

$$\rho_{12}^2 \leq \left(\frac{\sqrt{\Gamma(2H_1 + 1) \Gamma(2H_2 + 1)} \sqrt{\sin(H_1\pi) \sin(H_2\pi)}}{\Gamma(H_1 + H_2 + 1) \sin \left(\frac{(H_1 + H_2)\pi}{2} \right)} \right)^2 \quad (C10)$$

is the one present in the literature⁵² that guarantees the proper covariance structure.

Appendix D: Proof of Theorem 3, spectral content of the increment process of 2D fBm

Proof. First, following⁵², we know the spectral representation of the increments

$$\Delta \mathbf{Z}(n) \equiv \mathbf{Z}(n+1) - \mathbf{Z}(n) = \int_{\mathbb{R}} \frac{e^{i(n+1)x} - e^{inx}}{ix} \left(x_+^{-D} A + x_-^{-D} \overline{A} \right) \widehat{B}(dx), \quad (D1)$$

where A is given in Eq. (A10), $D = H - \frac{1}{2}I$ and \tilde{B} is Gaussian spectral measure with $\langle |\hat{B}(dx)|^2 \rangle = dx$ control measure. Now we can write

$$\begin{aligned} \langle \Delta \mathbf{Z}(k) \Delta \mathbf{Z}(0) \rangle &= \left\langle \int_{\mathbb{R}} \int_{\mathbb{R}} \frac{e^{i(k+1)x} - e^{ikx}}{ix} \overline{\left(\frac{e^{iy} - 1}{iy} \right)} \left(x_+^{-D} A + x_-^{-D} \overline{A} \right) \cdot \left(y_+^{-D} A + y_-^{-D} \overline{A} \right)^* \hat{B}(dx) \hat{B}^*(dy) \right\rangle \\ &= \int_{\mathbb{R}} \frac{e^{i(k+1)x} - e^{ikx}}{ix} \overline{\left(\frac{e^{ix} - 1}{ix} \right)} \left(x_+^{-D} A + x_-^{-D} \overline{A} \right) \cdot \left(x_+^{-D} A + x_-^{-D} \overline{A} \right)^* dx \\ &= \sum_{n=-\infty}^{\infty} \int_{-\pi+2n\pi}^{\pi+2n\pi} \frac{e^{i(k+1)x} - e^{ikx}}{ix} \overline{\left(\frac{e^{ix} - 1}{ix} \right)} \left(x_+^{-D} A + x_-^{-D} \overline{A} \right) \cdot \left(x_+^{-D} A + x_-^{-D} \overline{A} \right)^* dx \end{aligned}$$

substituting $x = f + 2n\pi$ and exchanging the integral and sum we obtain

$$\begin{aligned} &= \int_{-\pi}^{\pi} \sum_{n=-\infty}^{\infty} e^{ik(f+2n\pi)} \frac{|e^{i(f+2n\pi)} - 1|^2}{(f+2n\pi)^2} \left((f+2n\pi)_+^{-D} A + (f+2n\pi)_-^{-D} \overline{A} \right) \cdot \left((f+2n\pi)_+^{-D} A + (f+2n\pi)_-^{-D} \overline{A} \right)^* df \\ &= \int_{-\pi}^{\pi} e^{ikf} |e^{if} - 1|^2 \sum_{n=-\infty}^{\infty} \left((f+2n\pi)_+^{-D} A A^* (f+2n\pi)_+^{-D} + (f+2n\pi)_-^{-D} \overline{A} \overline{A}^* (f+2n\pi)_-^{-D} \right) / (f+2n\pi)^2 df. \end{aligned}$$

Remembering that $AA^* = C$ (elements of C are given in Eqs. (A11) and (C5)), and taking Remark 1.3.6 and 1.3.8⁵² we obtain the final result for the power spectral density of $\Delta \mathbf{Z}$.

Considering element-wise power spectral density, we have

$$\begin{aligned} S_{\Delta \mathbf{Z},jk}(f) &= |e^{if} - 1|^2 \sum_{n=-\infty}^{\infty} \left[(f+2n\pi)_+^{-(d_j+d_k)} c_{jk} + (f+2n\pi)_-^{-(d_j+d_k)} \overline{c_{jk}} \right] / (f+2n\pi)^2 \\ &= |e^{if} - 1|^2 \sum_{n=-\infty}^{\infty} \left[(f+2n\pi)_+^{-(H_j+H_k+1)} c_{jk} + (f+2n\pi)_-^{-(H_j+H_k+1)} \overline{c_{jk}} \right] / (f+2n\pi)^2, \end{aligned}$$

as $d_j = H_j - 1/2$.

Moreover, by simple calculations we have the asymptotics as $f \rightarrow 0$

$$S_{\Delta \mathbf{Z},jk}(f) \sim c_{jk} f^{-(H_j+H_k+1)}.$$

□

Appendix E: Proof of Theorem 4, spectral content of 2D fBm trajectory

Proof. Power spectral density for the trajectory $\mathbf{Z}(t), 0 \leq t \leq T$, is given by

$$S_{jk}(f, T) \equiv \frac{1}{T} \int_0^T e^{ift} Z_j(t) dt \overline{\int_0^T e^{ifs} Z_k(s) ds}. \quad (\text{E1})$$

It is a random variable depending both on the considered frequency f , time horizon T , and the trajectory $\mathbf{Z}(t)$. Since we want to consider the ensemble-averaged power spectral density, we have

$$\begin{aligned} \langle S_{jk}(f, T) \rangle &= \frac{1}{T} \left\langle \int_0^T e^{ift} Z_j(t) dt \overline{\int_0^T e^{ifs} Z_k(s) ds} \right\rangle = \text{[by Fubini theorem]} \\ &= \frac{1}{T} \int_0^T \int_0^T e^{if(t-s)} \langle Z_j(t) Z_k(s) \rangle dt ds \\ &= \frac{1}{T} \int_0^T \int_0^T e^{if(t-s)} \gamma_{jk}(t, s) dt ds, \end{aligned}$$

where $\gamma_{jk}(t, s)$ is the covariance function for Z_j and Z_k . For simplicity, we write the general form of this function with weighting function w_{jk} that has explicit form for both causal and well-balanced cases (Eq. (13)).

Here, we consider the case when $H_j + H_k \neq 1$ or the considered model is well-balanced 2D fBm (so that, there is no log part in the cross covariance function). By rescaling the integrals' variables $\frac{t}{T} \rightarrow x, \frac{s}{T} \rightarrow y$ and by introducing $\tilde{\omega} = fT$, we have

$$\langle S_{jk}(f, T) \rangle = T^{H_j+H_k+1} \frac{\sigma_j \sigma_k}{2} \int_0^1 \int_0^1 e^{i\tilde{\omega}(x-y)} \left(w_{jk}(x) x^{H_j+H_k} + w_{jk}(-y) y^{H_j+H_k} - w_{jk}(x-y) |x-y|^{H_j+H_k} \right) dx dy \quad (\text{E2})$$

We calculate each element separately. Let us introduce the notation

$$\text{II} \equiv \int_0^1 \int_0^1 e^{i\tilde{\omega}(x-y)} w_{jk}(x) x^{H_j+H_k} dy dx, \quad (\text{E3})$$

$$\text{III} \equiv \int_0^1 \int_0^1 e^{i\tilde{\omega}(x-y)} w_{jk}(-y) y^{H_j+H_k} dy dx, \quad (\text{E4})$$

$$\text{IIII} \equiv \int_0^1 \int_0^1 e^{i\tilde{\omega}(x-y)} w_{jk}(x-y) |x-y|^{H_j+H_k} dy dx. \quad (\text{E5})$$

Then the resulting integral is equal to

$$\langle S_{jk}(f, T) \rangle = T^{H_j+H_k+1} \frac{\sigma_j \sigma_k}{2} (\text{II} + \text{III} - \text{IIII}). \quad (\text{E6})$$

Let us start with II

$$\begin{aligned} \text{II} &\equiv \int_0^1 \int_0^1 e^{i\tilde{\omega}(x-y)} w_{jk}(x) x^{H_j+H_k} dy dx \\ &= \int_0^1 e^{i\tilde{\omega}x} \frac{1 - e^{-i\tilde{\omega}}}{i\tilde{\omega}} x^{H_j+H_k} \underbrace{w_{jk}(x)}_{\text{constant } \forall x > 0} dx \\ &= w_{jk}(1) \frac{1 - e^{-i\tilde{\omega}}}{i\tilde{\omega}} \left[\int_0^1 \cos(\tilde{\omega}x) + i \sin(\tilde{\omega}x) x^{H_j+H_k} dx \right]. \end{aligned}$$

Now, let us consider III

$$\begin{aligned} \text{III} &\equiv \int_0^1 \int_0^1 e^{i\tilde{\omega}(x-y)} w_{jk}(-y) y^{H_j+H_k} dx dy \\ &= \int_0^1 e^{-i\tilde{\omega}y} \frac{e^{i\tilde{\omega}} - 1}{i\tilde{\omega}} y^{H_j+H_k} \underbrace{w_{jk}(-y)}_{\text{constant } \forall y > 0} dy \\ &= w_{jk}(-1) \frac{e^{i\tilde{\omega}} - 1}{i\tilde{\omega}} \left[\int_0^1 \cos(\tilde{\omega}x) - i \sin(\tilde{\omega}x) y^{H_j+H_k} dx \right]. \end{aligned}$$

Summing up the first two parts, we have

$$\text{II} + \text{III} = \int_0^1 \cos(\tilde{\omega}x) x^{H_j+H_k} dx \left[w_{jk}(1) \frac{1 - e^{-i\tilde{\omega}}}{i\tilde{\omega}} - w_{jk}(-1) \frac{1 - e^{i\tilde{\omega}}}{i\tilde{\omega}} \right] \quad (\text{E7})$$

$$+ \int_0^1 \sin(\tilde{\omega}y) y^{H_j+H_k} dy \left[w_{jk}(1) \frac{1 - e^{-i\tilde{\omega}}}{i\tilde{\omega}} + w_{jk}(-1) \frac{1 - e^{i\tilde{\omega}}}{i\tilde{\omega}} \right]. \quad (\text{E8})$$

Reintroducing functions \mathcal{C}_{jk} and \mathcal{S}_{jk} as

$$\mathcal{C}_{jk} \equiv \mathcal{C}_{jk}(\tilde{\omega}) = \int_0^1 \cos(\tilde{\omega}x) x^{H_j+H_k} dx, \quad (\text{E9})$$

$$\mathcal{S}_{jk} \equiv \mathcal{S}_{jk}(\tilde{\omega}) = \int_0^1 \sin(\tilde{\omega}x) x^{H_j+H_k} dx, \quad (\text{E10})$$

and utilizing that $w_{jk}(x) = \rho_{jk} - \text{sign}(x)\eta_{jk}$ we can simplify the expression

$$\begin{aligned} \text{II} + \text{III} &= \mathcal{C}_{jk} \left[(\rho_{jk} - \eta_{jk}) \frac{1 - \cos(\tilde{\omega}) + i \sin(\tilde{\omega})}{i\tilde{\omega}} - (\rho_{jk} + \eta_{jk}) \frac{1 - \cos(\tilde{\omega}) - i \sin(\tilde{\omega})}{i\tilde{\omega}} \right] \\ &\quad + \mathcal{S}_{jk} \left[(\rho_{jk} - \eta_{jk}) \frac{1 - \cos(\tilde{\omega}) + i \sin(\tilde{\omega})}{i\tilde{\omega}} - (\rho_{jk} + \eta_{jk}) \frac{1 - \cos(\tilde{\omega}) - i \sin(\tilde{\omega})}{i\tilde{\omega}} \right] \\ &= 2\rho_{jk} \left(\frac{\sin \tilde{\omega}}{\tilde{\omega}} \mathcal{C}_{jk} + \frac{1 - \cos \tilde{\omega}}{\tilde{\omega}} \mathcal{S}_{jk} \right) + 2i\eta_{jk} \left(\frac{1 - \cos \tilde{\omega}}{\tilde{\omega}} \mathcal{C}_{jk} - \frac{\sin \tilde{\omega}}{\tilde{\omega}} \mathcal{S}_{jk} \right) \end{aligned} \quad (\text{E11})$$

For the third part, we have

$$\begin{aligned}
\text{III} &\equiv \int_0^1 \int_0^1 e^{i\tilde{\omega}(x-y)} w_{jk}(x-y) |x-y|^{H_j+H_k} dx dy = \quad |\text{substitute } u = x-y, z = x| \\
&= \int_{-1}^0 du \int_0^{u+1} dz w_{jk}(u) e^{i\tilde{\omega}u} |u|^{H_j+H_k} + \int_0^1 du \int_u^1 dz w_{jk}(u) e^{i\tilde{\omega}u} u^{H_j+H_k} \\
&= \int_{-1}^0 du w_{jk}(u) e^{i\tilde{\omega}u} |u|^{H_j+H_k} (1+u) + \int_0^1 du w_{jk}(u) e^{i\tilde{\omega}u} u^{H_j+H_k} (1-u) \\
&= \int_0^1 du \underbrace{w_{jk}(-u)}_{=\rho_{jk}+\eta_{jk}} e^{-i\tilde{\omega}u} u^{H_j+H_k} (1-u) + \int_0^1 du \underbrace{w_{jk}(u)}_{=\rho_{jk}-\eta_{jk}} e^{i\tilde{\omega}u} u^{H_j+H_k} (1-u) \\
&= \rho_{jk} \int_0^1 \underbrace{(e^{-i\tilde{\omega}u} + e^{i\tilde{\omega}u})}_{=2\cos(\tilde{\omega}u)} u^{H_j+H_k} (1-u) du - \eta_{jk} \int_0^1 \underbrace{(e^{i\tilde{\omega}u} - e^{-i\tilde{\omega}u})}_{=2i\sin(\tilde{\omega}u)} u^{H_j+H_k} (1-u) du \\
&= 2\rho_{jk} \left(C_{jk} - \int_0^1 \cos(\tilde{\omega}u) u^{H_j+H_k+1} du \right) - 2i\eta_{jk} \left(S_{jk} - \int_0^1 \sin(\tilde{\omega}u) u^{H_j+H_k+1} du \right).
\end{aligned}$$

We see that

$$\int_0^1 \cos(\tilde{\omega}u) u^{H_j+H_k+1} du = \frac{d}{d\tilde{\omega}} \int_0^1 \sin(\tilde{\omega}u) u^{H_j+H_k} du = \frac{d}{d\tilde{\omega}} S_{jk}, \quad (\text{E12})$$

$$\int_0^1 \sin(\tilde{\omega}u) u^{H_j+H_k+1} du = -\frac{d}{d\tilde{\omega}} \int_0^1 \cos(\tilde{\omega}u) u^{H_j+H_k} du = -\frac{d}{d\tilde{\omega}} C_{jk}, \quad (\text{E13})$$

or, via integration by parts we obtain

$$\int_0^1 \cos(\tilde{\omega}u) u^{H_j+H_k+1} du = \frac{\sin \tilde{\omega}}{\tilde{\omega}} - \frac{H_j + H_k + 1}{\tilde{\omega}} S_{jk}, \quad (\text{E14})$$

$$\int_0^1 \sin(\tilde{\omega}u) u^{H_j+H_k+1} du = \frac{-\cos \tilde{\omega}}{\tilde{\omega}} + \frac{H_j + H_k + 1}{\tilde{\omega}} C_{jk}. \quad (\text{E15})$$

We then arrive at the final expression

$$\begin{aligned}
\text{II} + \text{III} - \text{III} &= 2\rho_{jk} \left(\left[\frac{\sin \tilde{\omega}}{\tilde{\omega}} - 1 \right] C_{jk} + \frac{1 - \cos \tilde{\omega}}{\tilde{\omega}} S_{jk} + \frac{d}{d\tilde{\omega}} S_{jk} \right) \\
&\quad + 2i\eta_{jk} \left(\frac{1 - \cos \tilde{\omega}}{\tilde{\omega}} C_{jk} - \left[\frac{\sin \tilde{\omega}}{\tilde{\omega}} + 1 \right] S_{jk} - \frac{d}{d\tilde{\omega}} C_{jk} \right), \quad (\text{E16})
\end{aligned}$$

or equivalently

$$\begin{aligned}
\text{II} + \text{III} - \text{III} &= 2\rho_{jk} \left(\left[\frac{\sin \tilde{\omega}}{\tilde{\omega}} - 1 \right] C_{jk} + \frac{1 - \cos \tilde{\omega} - H_j - H_k - 1}{\tilde{\omega}} S_{jk} + \frac{\sin \tilde{\omega}}{\tilde{\omega}} \right) \\
&\quad + 2i\eta_{jk} \left(\frac{1 - \cos \tilde{\omega} + H_j + H_k + 1}{\tilde{\omega}} C_{jk} - \left[\frac{\sin \tilde{\omega}}{\tilde{\omega}} + 1 \right] S_{jk} \right). \quad (\text{E17})
\end{aligned}$$

□

Appendix F: Proof of [Theorem 5](#), asymptotics of ensemble-averaged PSD

Proof. Per¹⁶ we have the asymptotic behaviour of functions C_{jk} and S_{jk}

$$C_{jk}(\tilde{\omega}) \simeq \frac{a_{jk}}{\tilde{\omega}^{H_j+H_k+1}} + \frac{\sin \tilde{\omega}}{\tilde{\omega}} + \frac{(H_j + H_k) \cos \tilde{\omega}}{\tilde{\omega}^2} + \frac{(H_j + H_k)(1 - H_j - H_k) \sin \tilde{\omega}}{\tilde{\omega}^3} + O\left(\frac{1}{\tilde{\omega}^4}\right), \quad (\text{F1})$$

$$S_{jk}(\tilde{\omega}) \simeq \frac{a_{jk} \tan\left(\frac{\pi(H_j+H_k)}{2}\right)}{\tilde{\omega}^{H_j+H_k+1}} - \frac{\cos \tilde{\omega}}{\tilde{\omega}} + \frac{(H_j + H_k) \sin \tilde{\omega}}{\tilde{\omega}^2} - \frac{(H_j + H_k)(1 - H_j - H_k) \cos \tilde{\omega}}{\tilde{\omega}^3} + O\left(\frac{1}{\tilde{\omega}^4}\right), \quad (\text{F2})$$

where $a_{jk} = \Gamma(H_j + H_k) \sin\left(\frac{\pi}{2}(H_j + H_k)\right)$.

Thus, grouping the elements by their powers, we have (as $\tilde{\omega} \rightarrow \infty$)

$$\Re\langle S_{jk}(\tilde{\omega}, T) \rangle \simeq T^{H_j+H_k+1} \sigma_j \sigma_k \rho_{jk} \left\{ \left[\frac{1}{\tilde{\omega}^2} - \frac{(H_j + H_k) \sin \tilde{\omega}}{\tilde{\omega}^3} + O\left(\frac{1}{\tilde{\omega}^4}\right) \right] \right. \quad (\text{F3})$$

$$\left. + \frac{a_{jk}}{\tilde{\omega}^{H_j+H_k+1}} \left[1 - \frac{(H_j + H_k + \cos \tilde{\omega}) \cot\left(\frac{\pi(H_j+H_k)}{2}\right)}{\tilde{\omega}} \right] \right\}, \quad (\text{F4})$$

$$\Im\langle S_{jk}(\tilde{\omega}, T) \rangle \simeq T^{H_j+H_k+1} \sigma_j \sigma_k \eta_{jk} \left\{ \left[\frac{2}{\tilde{\omega}^2} - \frac{(H_j + H_k) \cos \tilde{\omega} (3 - \cos \tilde{\omega})}{\tilde{\omega}^3} + O\left(\frac{1}{\tilde{\omega}^4}\right) \right] \right. \quad (\text{F5})$$

$$\left. + \frac{a_{jk}}{\tilde{\omega}^{H_j+H_k+1}} \left[\cot\left(\frac{\pi(H_j + H_k)}{2}\right) - \frac{2 + H_j + H_k - \cos \tilde{\omega} + \sin \tilde{\omega} \cot\left(\frac{\pi(H_j+H_k)}{2}\right)}{\tilde{\omega}} \right] \right\}.$$

□

REFERENCES

- ¹Ralf Metzler, Jae-Hyung Jeon, Andrey G Cherstvy, and Eli Barkai. Anomalous diffusion models and their properties: non-stationarity, non-ergodicity, and ageing at the centenary of single particle tracking. *Physical Chemistry Chemical Physics*, 16(44):24128–24164, 2014.
- ²Diego Krapf. Mechanisms underlying anomalous diffusion in the plasma membrane. *Current Topics in Membranes*, 75:167–207, 2015.
- ³Carlo Manzo and Maria F. Garcia-Parajo. A review of progress in single particle tracking: from methods to biophysical insights. *Reports on Progress in Physics*, 78(12):124601, 2015.
- ⁴Hao Shen, Lawrence J Tausin, Rashad Baiyasi, Wenxiao Wang, Nicholas Moringo, Bo Shuang, and Christy F Landes. Single particle tracking: from theory to biophysical applications. *Chemical Reviews*, 117(11):7331–7376, 2017.
- ⁵Michał Balcerek, Samudrajit Thapa, Krzysztof Burnecki, Holger Kantz, Ralf Metzler, Agnieszka Wyłomańska, and Aleksei Chechkin. Multifractional Brownian motion with telegraphic, stochastically varying exponent. *Phys. Rev. Lett.*, 134:197101, 2025.
- ⁶Vasiliki Plerou, Parameswaran Gopikrishnan, Luís A Nunes Amaral, Xavier Gabaix, and H Eugene Stanley. Economic fluctuations and anomalous diffusion. *Physical Review E*, 62(3):R3023, 2000.
- ⁷Gorka Muñoz-Gil et al. Objective comparison of methods to decode anomalous diffusion. *Nature Communications*, 12:6253, 2021.
- ⁸Albert Einstein. Über die von der molekularkinetischen Theorie der Wärme geforderte Bewegung von in ruhenden Flüssigkeiten suspendierten Teilchen. *Ann. Phys.*, 322:549, 1905.
- ⁹Andrei N Kolmogorov. Wienersche Spiralen und einige andere interessante Kurven in Hilbertscen Raum. *C.R. (Doklady) Acad. Sci. URSS (NS)*, 26:115, 1940.
- ¹⁰Benoit B Mandelbrot and John W Van Ness. Fractional Brownian Motions, Fractional Noises and Applications. *SIAM Review*, 10:422, 1968.
- ¹¹Mark M Meerschaert, David A Benson, and Boris Bäumer. Multidimensional advection and fractional dispersion. *Physical Review E*, 59(5):5026, 1999.
- ¹²Jae-Hyung Jeon and Ralf Metzler. Fractional Brownian motion and motion governed by the fractional Langevin equation in confined geometries. *Physical Review E—Statistical, Nonlinear, and Soft Matter Physics*, 81(2):021103, 2010.
- ¹³Frédéric Lavancier, Anne Philippe, and Donatas Surgailis. Covariance function of vector self-similar processes. *Statistics & Probability Letters*, 79(23):2415–2421, 2009.
- ¹⁴Pierre-Olivier Amblard, Jean-François Coeurjolly, Frédéric Lavancier, and Anne Philippe. Basic properties of the multivariate fractional Brownian motion. *arXiv preprint arXiv:1007.0828*, 2010.
- ¹⁵Grzegorz Sikora, Agnieszka Wyłomańska, Janusz Gajda, Laura Sole, Elizabeth J. Akin, Michael M. Tamkun, and Diego Krapf. Elucidating distinct ion channel populations on the surface of hippocampal neurons via single-particle tracking recurrence analysis. *Physical Review E*, 96:062404, 2017.

- ¹⁶Diego Krapf, Nils Lukat, Enzo Marinari, Ralf Metzler, Gleb Oshanin, Christine Selhuber-Unkel, Alessio Squarcini, Lorenz Stadler, Matthias Weiss, and Xinran Xu. Spectral content of a single non-Brownian trajectory. *Physical Review X*, 9(1):011019, 2019.
- ¹⁷Vittoria Sposini, Diego Krapf, Enzo Marinari, Raimon Sunyer, Felix Ritort, Fereydoon Taheri, Christine Selhuber-Unkel, Rebecca Benelli, Matthias Weiss, Ralf Metzler, and Gleb Oshanin. Towards a robust criterion of anomalous diffusion. *Communications Physics*, 5(1):305, 2022.
- ¹⁸Gorka Muñoz-Gil, Harshith Bachimanchi, Jesús Pineda, Benjamin Midtvedt, Maciej Lewenstein, Ralf Metzler, Diego Krapf, Giovanni Volpe, and Carlo Manzo. Quantitative evaluation of methods to analyze motion changes in single-particle experiments. *arXiv preprint arXiv:2311.18100*, 2023.
- ¹⁹Irena Bronstein, Yonatan Israel, Eldad Kepten, Sabine Mai, Yaron Shav-Tal, Eli Barkai, and Yuval Garini. Transient anomalous diffusion of telomeres in the nucleus of mammalian cells. *Physical Review Letters*, 103(1):018102, 2009.
- ²⁰Aleksander Weron, Krzysztof Burnecki, Elizabeth J Akin, Laura Solé, Michał Balcerek, Michael M Tamkun, and Diego Krapf. Ergodicity breaking on the neuronal surface emerges from random switching between diffusive states. *Scientific Reports*, 7(1):5404, 2017.
- ²¹Adal Sabri, Xinran Xu, Diego Krapf, and Matthias Weiss. Elucidating the origin of heterogeneous anomalous diffusion in the cytoplasm of mammalian cells. *Physical Review Letters*, 125(5):058101, 2020.
- ²²Barton A Smith, William R Clark, and Harden M McConnell. Anisotropic molecular motion on cell surfaces. *Proceedings of the National Academy of Sciences*, 76(11):5641–5644, 1979.
- ²³Sanaz Sadegh, Jenny L Higgins, Patrick C Mannion, Michael M Tamkun, and Diego Krapf. Plasma membrane is compartmentalized by a self-similar cortical actin meshwork. *Physical Review X*, 7(1):011031, 2017.
- ²⁴Ivan Voříšek and Eva Syková. Evolution of anisotropic diffusion in the developing rat corpus callosum. *Journal of Neurophysiology*, 78(2):912–919, 1997.
- ²⁵Silvia De Santis, Andrea Gabrielli, Marco Bozzali, Bruno Maraviglia, Emiliano Macaluso, and Silvia Capuani. Anisotropic anomalous diffusion assessed in the human brain by scalar invariant indices. *Magnetic resonance in medicine*, 65(4):1043–1052, 2011.
- ²⁶Nisha Pawar, Claudia Donth, and Matthias Weiss. Anisotropic diffusion of macromolecules in the contiguous nucleocytoplasmic fluid during eukaryotic cell division. *Current Biology*, 24(16):1905–1908, 2014.
- ²⁷Luc R Van Loon, Josep M Soler, Werner Müller, and Michael H Bradbury. Anisotropic diffusion in layered argillaceous rocks: a case study with Opalinus Clay. *Environmental Science & Technology*, 38(21):5721–5728, 2004.
- ²⁸Michał Balcerek, Adrian Pacheco-Pozo, Agnieszka Wyłomańska, Krzysztof Burnecki, and Diego Krapf. Two-dimensional Brownian motion with dependent components: Turning angle analysis. *Chaos: An Interdisciplinary Journal of Nonlinear Science*, 35(2), 2025.
- ²⁹Jay Weerawardena and Gillian Sullivan Mort. Investigating social entrepreneurship: A multidimensional model. *Journal of World Business*, 41(1):21–35, 2006.
- ³⁰Łukasz Bielak, Aleksandra Grzesiek, Joanna Janczura, and Agnieszka Wyłomańska. Market risk factors analysis for an international mining company. Multi-dimensional, heavy-tailed-based modelling. *Resources Policy*, 74:102308, 2021.
- ³¹Laura Sacerdote, Massimiliano Tamborrino, and Cristina Zucca. First passage times of two-dimensional correlated processes: Analytical results for the Wiener process and a numerical method for diffusion processes. *Journal of Computational and Applied Mathematics*, 296:275–292, 2016.
- ³²Roumen Tsekov and Eli Ruckenstein. Two-dimensional Brownian motion of atoms and dimers on solid surfaces. *Surface Science*, 344(1):175–181, 1995.
- ³³Amelia G. Nobile Antonio Di Crescenzo, Virginia Giorno and Serena Spina. First-exit-time problems for two-dimensional Wiener and Ornstein–Uhlenbeck processes through time-varying ellipses. *Stochastics*, 96(1):696–727, 2024.
- ³⁴Steven Kou and Haowen Zhong. First-passage times of two-dimensional Brownian motion. *Advances in Applied Probability*, 48(4):1045–1060, 2016.
- ³⁵Satish Iyengar. Hitting lines with two-dimensional Brownian motion. *SIAM Journal on Applied Mathematics*, 45(6):983–989, 1985.
- ³⁶Peter J. Thomas and Benjamin Lindner. Phase descriptions of a multidimensional Ornstein-Uhlenbeck process. *Physical Review E*, 99:062221, 2019.
- ³⁷Katarzyna Maraj-Zygmat, Aleksandra Grzesiek, Grzegorz Sikora, Janusz Gajda, and Agnieszka Wyłomańska

- mańska. Testing of two-dimensional Gaussian processes by sample cross-covariance function. *Chaos: An Interdisciplinary Journal of Nonlinear Science*, 33(7):073135, 2023.
- ³⁸Eva Möller, Bärbel Schack, Matthias Arnold, and Herbert Witte. Instantaneous multivariate eeg coherence analysis by means of adaptive high-dimensional autoregressive models. *Journal of Neuroscience Methods*, 105(2):143–158, 2001.
- ³⁹Nobuhiro Morishima. Complete modeling of multidimensional noise as a multivariate autoregressive process. *Annals of Nuclear Energy*, 18(12):697–704, 1991.
- ⁴⁰James H. Stock and Mark W. Watson. Vector autoregressions. *Journal of Economic Perspectives*, 15(4):101–115, 2001.
- ⁴¹Shiqing Ling and Michael McAleer. Asymptotic theory for a vector ARMA-GARCH model. *Econometric Theory*, 19(2):280–310, 2003. doi:10.1017/S0266466603192092.
- ⁴²Feng Zhang. An application of vector GARCH model in semiconductor demand planning. *European Journal of Operational Research*, 181(1):288–297, 2007.
- ⁴³Farid Boussama, Florian Fuchs, and Robert Stelzer. Stationarity and geometric ergodicity of BEKK multivariate GARCH models. *Stochastic Processes and their Applications*, 121(10):2331–2360, 2011.
- ⁴⁴Michael Peter Norton and Denis G Karczub. *Fundamentals of noise and vibration analysis for engineers*. Cambridge university press, 2003.
- ⁴⁵Holger Hennig, Ragnar Fleischmann, Anneke Fredebohm, York Hagmayer, Jan Nagler, Annette Witt, Fabian J Theis, and Theo Geisel. The nature and perception of fluctuations in human musical rhythms. *PLoS One*, 6(10):e26457, 2011.
- ⁴⁶Diego Krapf. Nonergodicity in nanoscale electrodes. *Physical Chemistry Chemical Physics*, 15(2):459–465, 2013.
- ⁴⁷David S Dean, Antonio Iorio, Enzo Marinari, and Gleb Oshanin. Sample-to-sample fluctuations of power spectrum of a random motion in a periodic Sinai model. *Physical Review E*, 94(3):032131, 2016.
- ⁴⁸Zachary R Fox, Eli Barkai, and Diego Krapf. Aging power spectrum of membrane protein transport and other subordinated random walks. *Nature Communications*, 12(1):6162, 2021.
- ⁴⁹Michał Balcerek, Agnieszka Wyłomańska, Krzysztof Burnecki, Ralf Metzler, and Diego Krapf. Modelling intermittent anomalous diffusion with switching fractional Brownian motion. *New Journal of Physics*, 25(10):103031, 2023.
- ⁵⁰Stilian A. Stoev and Murad S. Taqqu. How rich is the class of multifractional Brownian motions? *Stochastic Processes and their Applications*, 116(2):200–221, 2006.
- ⁵¹Jean-François Coeurjolly, Pierre-Olivier Amblard, and Sophie Achard. On multivariate fractional Brownian motion and multivariate fractional Gaussian noise. In *2010 18th European Signal Processing Conference*, pages 1567–1571. IEEE, 2010.
- ⁵²Vladas Pipiras and Murad S Taqqu. *Long-range dependence and self-similarity*, volume 45. Cambridge University Press, 2017.
- ⁵³Makoto Maejima and J. David Mason. Operator-self-similar stable processes. *Stochastic Processes and their Applications*, 54(1):139–163, 1994.
- ⁵⁴Gustavo Didier and Vladas Pipiras. Integral representations and properties of operator fractional Brownian motions. *Bernoulli*, 17(1):1–33, 2011.
- ⁵⁵Patrice Abry and Gustavo Didier. Wavelet estimation for operator fractional Brownian motion. *Bernoulli*, 24(2):895–928, 2018.
- ⁵⁶Jan Beran, Yuanhua Feng, Sucharita Ghosh, and Rafal Kulik. *Long-Memory Processes*. Springer, 2016.
- ⁵⁷Langford B White and Boualem Boashash. Cross spectral analysis of nonstationary processes. *IEEE Transactions on Information Theory*, 36(4):830–835, 2002.
- ⁵⁸Clive WJ Granger and Robert Engle. Applications of spectral analysis in econometrics. *Handbook of statistics*, 3:93–109, 1983.
- ⁵⁹Antônio M.G De Lima, Sylvain Lambert, Domingos Alves Rade, Emmanuel Pagnacco, and Leila Khalij. Fatigue reliability analysis of viscoelastic structures subjected to random loads. *Mechanical Systems and Signal Processing*, 43(1-2):305–318, 2014.
- ⁶⁰Gaetan Kerschen, Keith Worden, Alexander F Vakakis, and Jean-Claude Golinval. Past, present and future of nonlinear system identification in structural dynamics. *Mechanical systems and signal processing*, 20(3):505–592, 2006.
- ⁶¹Ruofan Wang, Jiang Wang, Haitao Yu, Xile Wei, Chen Yang, and Bin Deng. Power spectral density and coherence analysis of Alzheimer’s EEG. *Cognitive Neurodynamics*, 9(3):291–304, 2015.

- ⁶²AR Amiri-Simkooei. On the nature of GPS draconitic year periodic pattern in multivariate position time series. *Journal of Geophysical Research: Solid Earth*, 118(5):2500–2511, 2013.
- ⁶³Ryogo Kubo, Morikazu Toda, and Natsuki Hashitsume. *Statistical physics II: nonequilibrium statistical mechanics*, volume 31. Springer Science & Business Media, 2012.
- ⁶⁴Markus Niemann, Holger Kantz, and Eli Barkai. Fluctuations of 1/f noise and the low-frequency cutoff paradox. *Physical Review Letters*, 110(14):140603, 2013.
- ⁶⁵Diego Krapf, Enzo Marinari, Ralf Metzler, Gleb Oshanin, Xinran Xu, and Alessio Squarcini. Power spectral density of a single Brownian trajectory: what one can and cannot learn from it. *New Journal of Physics*, 20(2):023029, 2018.
- ⁶⁶Grace Chan and Andrew TA Wood. Simulation of stationary Gaussian vector fields. *Statistics and Computing*, 9(4):265–268, 1999.
- ⁶⁷Joanna Syroka and Ralf Toumi. Scaling and persistence in observed and modeled surface temperature. *Geophysical Research Letters*, 28(17):3255–3258, 2001.
- ⁶⁸Dorje C Brody, Joanna Syroka, and Mihail Zervos. Dynamical pricing of weather derivatives. *Quantitative finance*, 2(3):189, 2002.
- ⁶⁹MN Piacquadio Losada, Rafael Santiago Seoane, A de la Barra, and L Facundo Caram. Fractional Brownian motions and their multifractal analysis applied to Parana river flow. *arXiv preprint arXiv:2002.04532*, 2020.
- ⁷⁰Jon D Pelletier. Fractal behavior in space and time in a simplified model of fluvial landform evolution. *Geomorphology*, 91(3-4):291–301, 2007.
- ⁷¹R Fischer, Metin Akay, Paolo Castiglioni, and Marco Di Rienzo. Multi- and monofractal indices of short-term heart rate variability. *Medical and Biological Engineering and Computing*, 41(5):543–549, 2003.
- ⁷²Bernard Hoop, Melvin D Burton, and Homayoun Kazemi. Fractal noise in breathing. In *Bioengineering approaches to pulmonary physiology and medicine*, pages 161–173. Springer, 1996.
- ⁷³Izrail Solomonovich Gradshteyn and Iosif Moiseevich Ryzhik. *Table of integrals, series, and products*. Academic Press, 2014.